

NAVAL POSTGRADUATE SCHOOL

Monterey, California



THESIS

**PERFORMANCE ANALYSIS OF
IRTOOL RAY REFRACTION PROGRAM AND
COMPARISON TO LWKD AND PIRAM MARINE
BOUNDARY LAYER PROGRAMS**

by

Antonios Georgopoulos

DTIC QUALITY INSPECTED 4

December, 1998

Thesis Advisor:

Alfred W. Cooper

Approved for public release; distribution is unlimited.

19990219026

REPORT DOCUMENTATION PAGE

Form Approved
OMB No. 0704-0188

Public reporting burden for this collection of information is estimated to average 1 hour per response, including the time for reviewing instruction, searching existing data sources, gathering and maintaining the data needed, and completing and reviewing the collection of information. Send comments regarding this burden estimate or any other aspect of this collection of information, including suggestions for reducing this burden, to Washington headquarters Services, Directorate for Information Operations and Reports, 1215 Jefferson Davis Highway, Suite 1204, Arlington, VA 22202-4302, and to the Office of Management and Budget, Paperwork Reduction Project (0704-0188) Washington DC 20503.

1. AGENCY USE ONLY (Leave blank)

2. REPORT DATE
December 1998

3. REPORT TYPE AND DATES COVERED
Master's Thesis

4. TITLE AND SUBTITLE

PERFORMANCE ANALYSIS OF IRTOOL RAY REFRACTION PROGRAM
AND COMPARISON TO LWKD AND PIRAM MARINE BOUNDARY LAYER
PROGRAMS

5. FUNDING NUMBERS

6. AUTHOR(S)

Georgopoulos, Antonios

7. PERFORMING ORGANIZATION NAME(S) AND ADDRESS(ES)

Naval Postgraduate School
Monterey, CA 93943-5000

8. PERFORMING ORGANIZATION
REPORT NUMBER

9. SPONSORING / MONITORING AGENCY NAME(S) AND ADDRESS(ES)

10. SPONSORING / MONITORING
AGENCY REPORT NUMBER

11. SUPPLEMENTARY NOTES

The views expressed in this thesis are those of the author and do not reflect the official policy or position of the Department of Defense or the U.S. Government.

12a. DISTRIBUTION / AVAILABILITY STATEMENT

Approved for public release; distribution is unlimited.

12b. DISTRIBUTION CODE

13. ABSTRACT (maximum 200 words)

The prediction of mirage conditions by the IRTOOL engagement simulation program has been evaluated by comparison with experimental visible and IR observations extracted from the MAPTIP experiment data base. IRTOOL predictions have also been compared with the LWKD and PIRAM Boundary Layer programs for identical input conditions. For sensors located above about 20 meters the values of Minimum Mirage Range and Maximum Inter-Vision Range become inconsistent and all models show similar mirage threshold performance offset internally and from the measurements by approximately 1-3 km (5-20%). This may be related to uncertainties in the temperature profiles generated from Boundary Layer models. Variations of 2-4° C in Air Sea Temperature are insufficient to account for the observed deviations.

14. SUBJECT TERMS

Refraction, marine boundary layer, temperature profile, mirage.

15. NUMBER OF
PAGES
82

16. PRICE CODE

17. SECURITY
CLASSIFICATION OF
REPORT

Unclassified

18. SECURITY CLASSIFICATION OF
THIS PAGE

Unclassified

19. SECURITY CLASSIFI- CATION
OF ABSTRACT

Unclassified

20. LIMITATION OF
ABSTRACT

UL

Approved for public release; distribution is unlimited

PERFORMANCE ANALYSIS OF
IRTOOL RAY REFRACTION PROGRAM AND
COMPARISON TO LWKD AND PIRAM
MARINE BOUNDARY LAYER PROGRAMS

Antonios Georgopoulos
Lieutenant Junior Grade, Hellenic Navy
B.S., Hellenic Naval Academy, 1990

Submitted in partial fulfillment of the
requirements for the degree of

MASTER OF SCIENCE IN APPLIED PHYSICS

from the

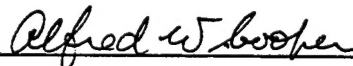
NAVAL POSTGRADUATE SCHOOL
December 1998

Author:

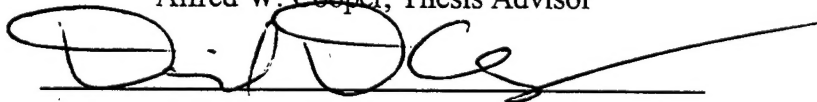


Antonios Georgopoulos

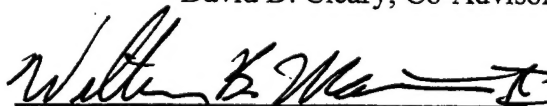
Approved by:



Alfred W. Cooper, Thesis Advisor



David D. Cleary, Co-Advisor



William B. Maier II, Chairman,
Department of Physics

ABSTRACT

The prediction of mirage conditions by the IRTOOL engagement simulation program has been evaluated by comparison with experimental visible and IR observations extracted from the MAPTIP experiment data base. IRTOOL predictions have also been compared with the LWKD and PIRAM Boundary Layer programs for identical input conditions. For sensors located above about 20 meters the values of Minimum Mirage Range and Maximum Inter-Vision Range become inconsistent and all models show similar mirage threshold performance offset internally and from the measurements by approximately 1-3 km (5-20%). This may be related to uncertainties in the temperature profiles generated from Boundary Layer models. Variations of 2-4° C in Air Sea Temperature are insufficient to account for the observed deviations.

TABLE OF CONTENTS

I.	INTRODUCTION.....	1
A.	BACKGROUND.....	1
B.	OBJECTIVES OF THE RESEARCH.....	2
C.	STRUCTURE.....	2
II.	ELECTROMAGNETIC WAVE PROPAGATION IN THE MARINE BOUNDARY LAYER.....	5
A.	INTRODUCTION.....	5
B.	REFRACTIVE INDEX OF AIR.....	5
C.	REFRACTION PHENOMENA IN THE MARINE BOUNDARY LAYER.....	12
D.	MIRAGE EFFECT.....	14
III.	IRTOOL MODEL.....	17
A.	INTRODUCTION.....	17
B.	IRTOOL CAPABILITIES.....	17
1.	Modules.....	18
2.	IRTOOL Outputs.....	19
3.	IRTOOL Operation.....	20
4.	Input Menu.....	21
5.	Job Description Submission.....	22
C.	USER MODULE.....	24
D.	MODEL ALGORITHMS.....	25
IV.	EXPERIMENTAL ARRANGEMENT AND PROCEDURE.....	29
A.	INTRODUCTION.....	29
C.	EXPERIMENTAL SETUP	29

V.	DATA ANALYSIS.....	35
A.	INTRODUCTION.....	35
B.	NPS ATMOSPHERE PROFILER.....	37
C.	DATA ANALYSIS	38
1.	Ship Tracking Event B.....	41
2.	Ship Tracking Event K.....	49
VI.	CONCLUSIONS	65
	LIST OF REFERENCES.....	69
	INITIAL DISTRIBUTION LIST.....	71

ACKNOWLEDGEMENT

I would like to thank my thesis advisor Professor A. W. Cooper for his help, patience and contribution to my thesis work. I am thankful to Dr. Luc Forand from DREV, for the provision of the data analyzed. I wish also to thank the Boundary Layer Studies Group of the Meteorology Department of the Naval Postgraduate School and especially its coordinator Professor Kenneth L. Davidson for the MBL program he provided and his advice on the meteorological aspects of the research.

This study was supported by the Naval Postgraduate School under the DFR Merit Program.

I would like also to acknowledge, the financial support of participation in MAPTIP by Johns Hopkins University APL (Fleet Systems) and by NCCOSC-NRaD, and the contribution of the other participants in the MAPTIP experiment.

Lastly, I want to thank my wife Pagona for her unending encouragement, support and understanding which enable me to complete this work and my studies in NPS successfully.

I. INTRODUCTION

A. BACKGROUND

Sea skimming missiles and low altitude flying aircraft are a continual threat for ships, and IRST (infrared search and track) systems are used as passive detectors for their detection and acquisition. Atmospheric parameters that vary considerably cause various phenomena which can affect the detection range performance of electro-optical systems against low altitude flying targets. Refraction, the most important of these, is observed mainly in the marine boundary layer. In this region of the atmosphere sudden changes of the meteorological parameters produce great deviation in the expected detection ranges.

The necessity for prediction of IRST systems effectiveness and simulation of their operation imposed the development of accurate models that are capable of calculating the height profiles of atmospheric parameters and performing ray tracing in the lower region of the atmosphere. Researchers from different countries have developed new models and improved existing ones in investigating the refractive limitations. Recently also several multinational measurement series and joint experiments were conducted to improve the modelling of electro-optic propagation and infrared imaging in the marine boundary layer. The correlation of experimental data with the model's predicted results is essential to determine which model is reliable in the greater possible range of input data combinations.

B. OBJECTIVES OF THE RESEARCH

The IRTOOL computer program was developed by Arete Corporation to assist in the design phase of the next generation IRST. A group of scientists from the Canadian Defence Research Establishment Valcartier (DREV) applied the IRTOOL program to data they obtained over Monterey Bay in the EOPACE measurements in 1996 and concluded that it did not predict mirages in cases in which they were found experimentally. This raises doubts about the refraction capabilities of the IRTOOL code.

The major objective of this project is to generate mirage conditions in IRTOOL and directly compare the input and output data sets of the IRTOOL ray refraction model with those of other Marine Boundary Layer programs such as DREV's L(W)WKD model [Ref.1] and the French CELAR's (Centre d'Electronique de l'Armement) PIRAM (Profils d'Indice de Refraction en Atmosphere Marine) model, using the same input conditions for all these models. The secondary objective of the project is the inclusion of new sensor models in IRTOOL including a generic common module FLIR, and new targets including ones appropriate to low flying missiles, which will allow for other operational studies using IRTOOL.

C. STRUCTURE

This report consists of six chapters: Introduction, Electromagnetic Wave Propagation in the Marine Boundary Layer, IRTOOL model, Experimental Arrangement and Procedure, Data Analysis and Conclusions.

The chapter, "Electromagnetic Wave Propagation in the Marine Boundary Layer" describes the behavior of electromagnetic waves and how they are affected by atmospheric parameters in the marine boundary layer. The refraction phenomena of sub-refraction, super-refraction and mirage are also described.

In the chapter "IRTOOL model" the IRTOOL computer program is presented and its critical elements are described, together with its features most used during this project. This chapter includes also a short tutorial on how to set up calculations in IRTOOL and a brief discussion of the algorithms included in the models to be compared.

The "Experimental Arrangement and Procedure" chapter describes the setup and measurements carried out by several national groups in the MAPTIP (Marine Aerosol Properties and Thermal Imager Performance) experiment [Ref.2, Ref.3] at Katwijk, Netherlands in 1993, which was our data source. This provides important information for the upcoming data analysis.

In the "Data Analysis" chapter the MAPTIP data are compared with the model's calculations and the different outputs are associated and evaluated. The data analyzed were provided by Dr. Forand from DREV, coordinator of the "Refractive Effects in the Visible and IR" workgroup during the MAPTIP experiment.

Finally, in the last chapter, "Conclusions," the objectives are listed again and the effectiveness of each model is discussed. Also recommendations are given for future experiments and for the development of new models.

II. ELECTROMAGNETIC WAVE PROPAGATION IN THE MARINE BOUNDARY LAYER

A. INTRODUCTION

The surface layer of the marine atmosphere can influence IR sensing of distant low altitude targets. That region of the atmosphere, called the Marine Boundary Layer (MBL), extends from the sea surface to a height which may vary from twenty to several hundred meters [Ref.1]. The atmospheric effects in the MBL that are primarily responsible for limiting sensor performance are the following [Ref.4]:

1. ray refraction
2. turbulent distortion
3. atmospheric extinction.

The most significant of these factors is atmospheric refraction, which is due to the gradient of the atmosphere's refractive index. As a consequence of the refractive index variation, the combination of sub-refraction and super-refraction generates the mirage effect [Ref.5].

B. REFRACTIVE INDEX OF AIR

Electromagnetic energy propagates through the atmosphere in the form of waves which spread out spherically near the source and as plane waves further from the source. A ray is defined as the perpendicular to the wave front, or as defined in [Ref.6], "a line

drawn in space corresponding to the direction of flow of radiant energy.” As the waves propagate, an interaction takes place with the atmosphere. The extent of this interaction depends on the composition of the medium, the atoms and molecules of the atmosphere’s various gases. A fraction of the propagating energy is absorbed, another fraction is scattered and the rest is finally transmitted. For a homogeneous medium the phase velocity is given in m/sec by the following form [Ref.6]

$$v = \frac{1}{\sqrt{\epsilon\mu}} \quad (1)$$

where ϵ is the electric permittivity in $s^2 C^2/m^3 kg$ and μ is the permeability in $m kg/C^2$ of the medium. Given that the phase velocity in the vacuum, c , is

$$c = \frac{1}{\sqrt{\epsilon_0\mu_0}} \quad (2)$$

where ϵ_0 is the electric permittivity of free space and μ_0 is the permeability of free space, and that μ and μ_0 are equal for most materials, relation (1) becomes

$$v = \frac{c}{\sqrt{K_e}} \quad (3)$$

where $K_e = \epsilon/\epsilon_0$ is the dielectric constant of the medium.

The index of refraction n , is a dimensionless parameter directly connected to the

propagation speed in the medium and is given by the following form

$$n = \frac{c}{v} \quad (4)$$

which following (3) becomes

$$n = \sqrt{K_e} \quad (5)$$

It depends on the properties of the medium, the wavelength of the electromagnetic wave and usually is larger for a shorter wavelength than for a longer one [Ref.6].

The variation of the atmospheric properties across the path of a ray results in the bending of the ray, a phenomenon called refraction. If we consider a ray of monochromatic light incident at a plane surface separating two homogeneous media, a portion of the beam is reflected in the interface surface, remaining in the incidence medium, while the rest is transmitted downwards through the second medium. The reflected ray lies in the plane of incidence and according to the law of reflection, the incidence angle is equal to the reflection angle. Also, the refracted ray lies in the incidence plane and alters its direction as indicated by Snell's law

$$\frac{n_1}{n_2} = \frac{\sin \theta_2}{\sin \theta_1} \quad (6)$$

where θ_1 and θ_2 are the angles, with respect to the normal at the surface separating the two media, at which the incident ray strikes the surface and the refracted ray travels in the second medium, respectively. The rays bend towards the medium with higher refractive index or

opposite to the medium with the greater propagation speed. Figure 1 shows a ray passing through a multi-layered medium, whose refractive index is constant for each layer and

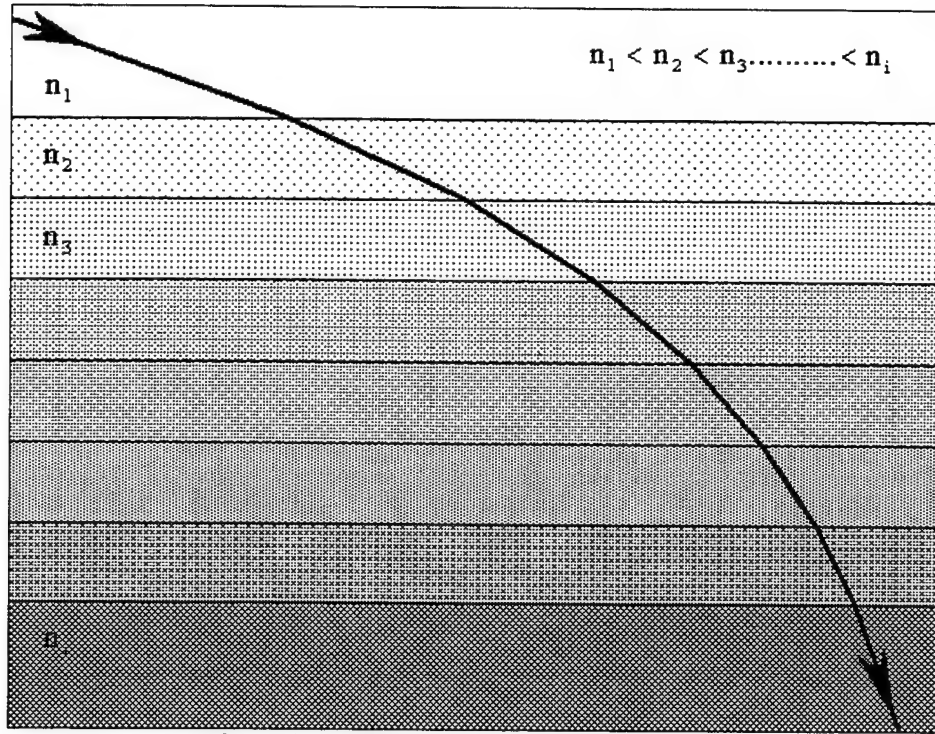


Figure1. Refracted ray in a layered medium.

increases downwards. A ray in a homogeneous isotropic medium where the refractive index is constant, will not bend but it will remain straight. One limiting factor for the detection range for an electromagnetic wave propagating in the atmosphere is absorption. However, if we consider a non-refractive atmosphere this detection range is additionally limited by the earth's curvature. For known target and sensor heights, the horizon-limited range (HLR) is given in km by the following form [Ref.7]:

$$\text{HLR} = \sqrt{2a} \left[\sqrt{h_s} + \sqrt{h_t} \right] \cdot 10^{-3} \quad (7)$$

Where h_s is the sensor height in meters

h_t is the target height in meters and

a is the earth radius in meters ($a = 6370000\text{m}$)

Lets now examine the impact of the refractive index and its gradient in the propagation path. We consider a beam of light propagating through a slightly inhomogeneous atmosphere as shown in Figure 2.

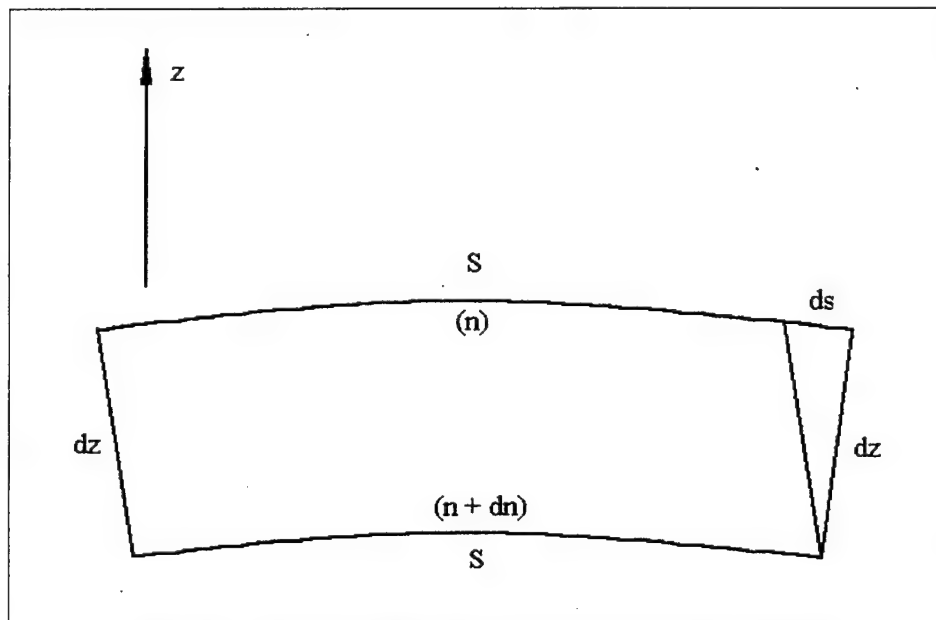


Figure 2. Ray bending in the atmosphere [After Ref.8]

The z-axis is perpendicular to the beam and both z-axis and the beam are contained in the same plane. Both the lower and the upper rays that are separated transversely by a distance of dz , correspond to index of refraction equal to $n+dn$ for the former and n for the latter. The lower ray travels a distance shorter by ds than the upper one does in the same period of time, because it travels in a greater index of refraction and consequently has smaller

propagation velocity. The result is the bending of the beam towards the direction of higher refractive index. According to Fermat's principle the optical path that each ray travels is stationary with respect to variations of that path [Ref.6]. Hence [Ref..9]

$$\frac{d}{dz}(ns) = n \frac{ds}{dz} + s \frac{dn}{dz} = 0 \Rightarrow s \frac{dz}{ds} = -n \frac{dz}{dn} \quad (8)$$

The change in the direction of the wave-front a along its path is ds/dz and the radius of bending will be

$$R = \frac{s}{ds/dz} \quad (9)$$

and finally following (8) the ray radius becomes

$$R = -n \frac{dz}{dn} = -n \frac{1}{(dn/dz)} \quad (10)$$

Since n in the lower region of the atmosphere is approximately equal to 1, relation (10) becomes

$$R = -\frac{1}{(dn/dz)} \quad (11)$$

So in the most usual case that the rays pass through a non-homogeneous atmosphere, they will follow a curved path with curvature $(1/R)$ proportional to the refractive index gradient.

In the case of Figure 2 our convention is that a negative refractive index gradient produces a positive radius of curvature and the rays bend downwards in the direction of the higher refractive index. The refractive index gradient dn/dz is in a direction perpendicular to the ray. Because in the visible and IR wavelengths the path of EM waves is governed by the vertical gradient [Ref.7], for the case of atmospheric refraction assuming that an optical ray travels perfectly horizontally, its path will be affected only by the vertical refractive index gradient.

The refractive index in the marine boundary layer changes rapidly with height. The atmospheric parameters that vary significantly and determine the refractive index gradient are the atmospheric pressure, the air temperature and the partial pressures of the atmosphere's various gases [Ref.3]. In the IR and the visible, the most significant of these gases, water vapor, is not a critical factor. In that case the refractive index gradient is given by the following formula [Ref. 9]:

$$n - 1 = \frac{77.6 p}{T} \left(1 + \frac{0.0075}{\lambda^2} \right) \cdot 10^{-6} \quad (12)$$

where p is atmospheric pressure in millibars, T is the air temperature in Kelvin and λ is the wavelength in micrometers. It can be shown that the refractive index gradient of air is inversely proportional to the temperature gradient and therefore, a positive or negative temperature gradient corresponds to a negative or positive refractive index gradient [Ref.3, Ref.7].

Since a typical value for the index of refraction is 1.0003 to 1.0004, another parameter has been defined for use. The refractivity N given by the following relation

$$N=(n-1)10^6 \quad (13)$$

is the “scaled up” index of refraction [Ref.10]. Consequently, the relationship between n and N is [Ref.11]

$$\frac{dN}{dz} = 10^6 \left(\frac{dn}{dz} \right) \quad (14)$$

C. REFRACTION PHENOMENA IN THE MARINE BOUNDARY LAYER

A positive vertical index gradient in the marine boundary layer results in sub-refraction conditions during which the optical rays bend with curvature opposite to the earth radius causing the distance to the horizon and the maximum inter-vision range to decrease. Figure 3 shows a number of rays propagating in the atmosphere under sub-refractive conditions. Maximum inter-vision range (MIVR) is “the absolute detection range limit imposed by refraction for a given sensor and target height”[Ref.7]. As the refractive index gradient is associated with the temperature gradient, sub-refraction occurs whenever this gradient is negative. Such meteorological conditions are met frequently in the open sea or in coastal waters as soon as the wind direction is from the open sea. Unlike the previous case, positive temperature gradient creates super-refraction. Super-refraction doesn’t occur often; it is uncommon for the temperature gradient to be positive, something that happens eventually

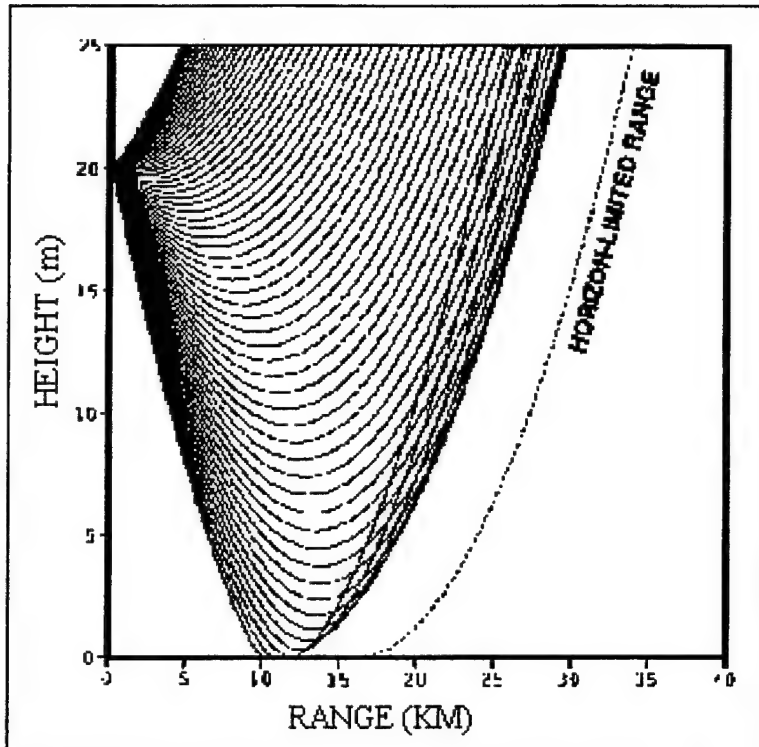


Figure 3. Sub-refraction [From Ref.7]

in coastal waters when warm continental air blows over the cold sea. If that is the case, the rays bend towards the earth causing radiation to propagate beyond the geometrical horizon.[Ref.7]. Figure 4 shows a number of rays propagating in the atmosphere under super-refractive conditions.

A term that will be used repeatedly in the following chapters is the air-to-sea temperature difference (ASTD). It is obvious that a positive ASTD corresponds to a negative refractive index gradient and produces super-refraction while a negative ASTD produces sub-refraction. In the case of ASTD close to zero the factor that determines the refractive index

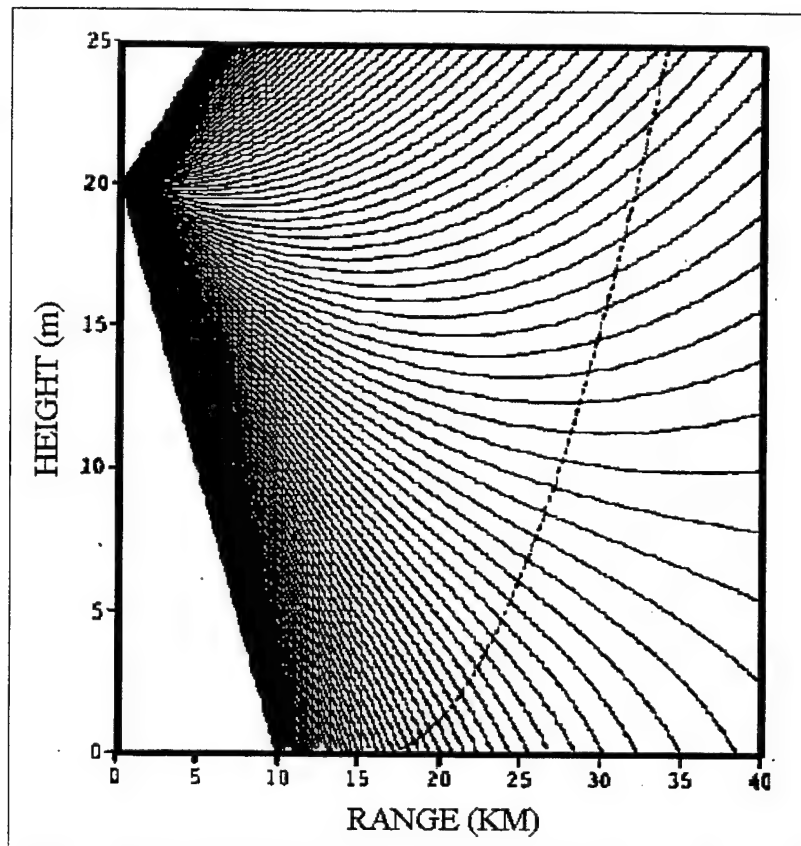


Figure 4. Super-refraction [from Ref.7]

is the atmospheric pressure gradient which is almost always negative. Thus the atmosphere is slightly super-refractive.

D. MIRAGE EFFECT

The elevation angle of an object as seen by an observer in the refractive atmosphere isn't the straight line connecting them, but the tangent at the observer of the refracted ray. The combination of sub-refraction with normal refraction or super-refraction in the marine boundary layer causes the mirage effect. During this phenomenon rays near the sea surface

are sub-refracted and bend upwards due to the positive index gradient. Meanwhile other rays from the same object following a different path pass higher than the first ones, are super-refracted or not refracted at all due to a negative or almost zero index gradient and bend downwards. Finally the observer sees the same object at two different elevation angles as shown in figure 5.

Another term that will be used often in the following chapters is the Minimum Mirage Range (MMR). The MMR is defined as “the minimum range at which a mirage (if there is one) of a particular visible/IR source begins to be observed”[Ref.2].

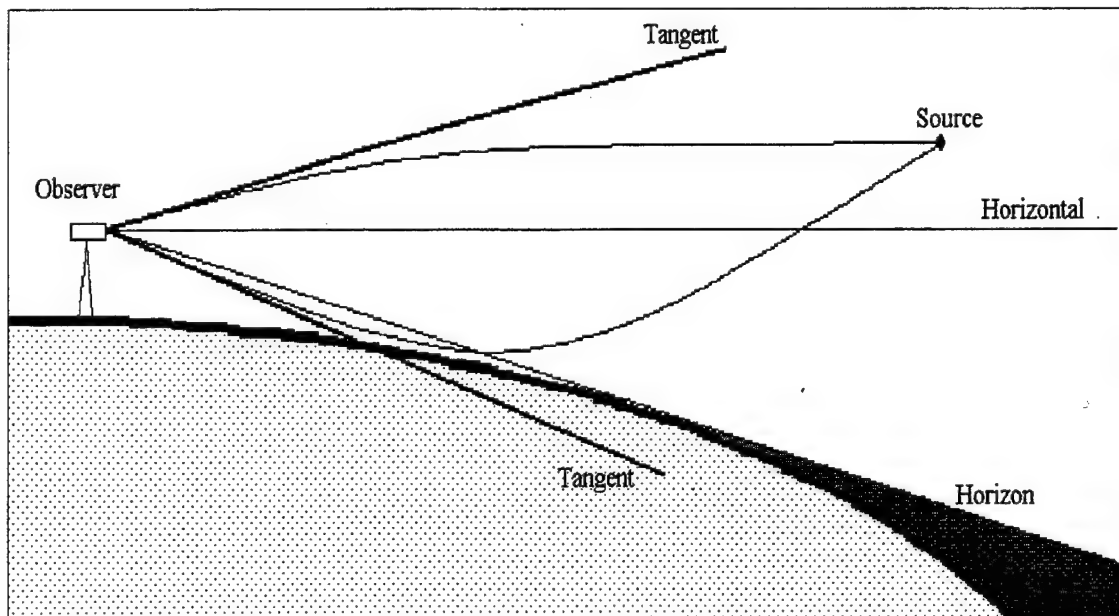


Figure 5. Mirage: the source is seen by the observer as two images [After Ref.3]

III. IRTOOL MODEL

A. INTRODUCTION

The IRTOOL Computer program is a simulation/computation model developed by Arete Associates and NSWC under the sponsorship of the Office of Naval Research in support of the Infrared Analysis Modelling and Measurements Program (IRAMMP)[Ref.14]. It uses a number of component models from various sources combined into a unified package that produces both visual simulations and engineering calculations for scenarios appropriate to the Infrared Search and Track system. Among other features, IRTOOL is capable of generating simulated scenes and animations of the target approach in addition to its surrounding environment (sea, sky and clouds), modelling system performance, performing data analysis, and supporting detection and tracking algorithm development[Ref.14]. The following sections form a brief tutorial for the program which emphasises the major components of IRTOOL regarding this thesis, presenting their features, the required inputs and critical details for the sufficient use of it. The last section discusses briefly the algorithms incorporated in the IRTOOL, L(W)WKD and PIRAM models.

B. IRTOOL CAPABILITIES

The main elements of IRTOOL are the modules. The modules are autonomous programs with determined inputs that can be combined so as to produce the desired outputs. The modules may be executed in a standard order or one selected by the user.

1. Modules

The most frequently used modules during this research were the Atmosphere Profiler, the Atmosphere Effects, the Engagement, the Target Injection, the Scene Simulation and the Sensor Effects Modules.

The Atmosphere Profiler Module generates height profiles of atmospheric parameters used by other modules and a LOWTRAN file which is used by the Atmosphere Effects and Sky Radiance Modules. The meteorological parameters used by the module are air temperature, sea temperature, relative humidity, and wind speed. The model assumes that the atmosphere is homogeneous in the horizontal direction, because the vertical gradients of the atmospheric parameters dominate over the horizontal. The vertical profiles generated can be modified when particular meteorological phenomena that can not be predicted, such as temperature inversion, are present or when the user wants to investigate the behavior of some atmospheric profile generated by another marine boundary layer program. The Atmosphere Shaper IDL routine in the Toolbox is assigned to help the user produce this custom profile.

The Engagement module generates a description of the target position, velocity at any moment since the start of the trajectory, and other relevant target orbit information used by other IRTOOL modules in their target modeling.

The Atmosphere Effects module uses the atmospheric profile to calculate ray refraction and add path radiance, transmissivity and atmospheric distortion parameters for each passband for the scene and the target [Ref.14]. The executed ray tracing calculations produce information about maximum inter-vision range, target magnification effects and the

target orientation in the sensor field of view. The Atmosphere effects module also generates mirage under the appropriate atmospheric conditions and sensor and target positions.

The Target injection module inserts point targets or results of the target signature module into a background which can be either simulated or stored data from actual measurements [Ref.14]. The user can test and evaluate signal processing and track algorithms using the scenes with injected targets generated by the module. The module can also apply atmospheric MTF to the injected targets and model the scintillation of the target due to atmospheric turbulence. The Target injection module requires, as input, the output from the target signature, scintillation, atmosphere effects, engagement and sensor module runs.

2. IRTOOL Outputs

The IRTOOL modules generate outputs that are line plot files or image data files. The line plot files have the file name extension ".plt" and they are ASCII text files. The user can create the desired plots by the Plot Curves command under the output menu. This command will launch an IDL routine used to create, display and print line plots. These line plot files are organized in several blocks of data. Each block of data contains the same number of columns and lists information for different passbands or target solutions. These output files can be read also by programs capable of reading ASCII data arranged in columns such as Microsoft Excel and Spyglass Plot.

The image data files are in HDF format, a public domain format supported by the National Center of Supercomputing Applications, University of Illinois[Ref.14]. They have

the file name extension ".img" and can be displayed and printed by the Display Images command under the output menu. The Compare images and the Animation commands are used under the same menu, the former to display and analyze two images and the later to create an animation from the sequenced image data files. The previous commands launch IDL routines that work with the HDF format which is also supported by other programs such as Spyglass Plot.

Some more IRTOOL output files such as log (file name extension ".log") and error (file name extension ".err") files or even the line plot files can be displayed using a text viewer launched by the Display text command under the menu output.

3. IRTOOL Operation

After launching IRTOOL the user can access IRTOOL's capabilities from the main menu bar at the top of the IRTOOL window. This menu bar consists of six pull down menus. With the first menu, "file," the user chooses, or creates if it doesn't exist, the working directory. IRTOOL will create a subdirectory to store the input data parameters and will place the output results there. The program status line just below the menu bar at the top of the IRTOOL window displays the working directory.

From the "Run" menu the user organizes the way that the desired operations and calculations will be executed. Each sequence of operations, involving a number of memory-stored input parameters, that is executed by IRTOOL is called a run script. A job script consists of a separate run script or a combination of several run scripts. The Run menu

dialogues allow the user to create a run script appropriate for the output he/she wants. We can produce a run script by choosing either a selected default run script, create an advanced run script, or create any order run script under the run menu. If we select the default run script command, IRTOOL displays a list of calculations that are most commonly needed. Among these results, sensor modeling, estimates of system performance, atmosphere modeling, and scene simulation are included.

After selecting a default run script the user can display a list of the required input parameters, needed for the right execution of the assigned modules, by clicking on Inputs. He/she can also check which modules will be executed before the submission of the job script by going to the Create Advance Run Script menu option.

By choosing the command Create Advanced Run Script or Create Any Order Run Script the driver executes a list of modules in an order shown in the corresponding window. In that case we must consider the interdependencies of IRTOOL, because some modules require as inputs some of the outputs from other module runs.

4. Input Menu

From the Input menu the user can edit and save groups of inputs, or load groups of IRTOOL input parameters used in previous runs. These parameters are divided into groups regarding their subject or dependency for easier access and customizing. The user, after reviewing the inputs needed for the selected run script, enters them using the input menu, organized by subject. For each group of parameters we can edit the parameters currently in

memory or load and edit a set of default values or a set that was previously saved or used in previous runs. When the user selects a run script the program first creates the subdirectory "Autosave" and then saves in it the input parameters automatically for easier access. The user can load all the inputs from a previous run by using the "LoadAll" command under the File menu. He/she can also use the "SaveAll" command under the File menu to store every parameter in memory or the Save command in each input dialogue to save only its contents. After editing the needed inputs the user can display all of them in a text window from the Input menu.

Another very helpful option that saves much time is the Advance Flow Control dialogue. It is essential to use it when only a small number of parameters is changing, and the user intends to do an extended number of simulations or apply outputs generated during previous runs.

A critical input parameter for the correct execution of the program is the number of trajectory points in the Output control window under the Input target trajectory parameters dialogue. This parameter affects the number of points along the trajectory at which results are calculated as well as the execution time of the atmosphere and scintillation modules; it must be over 100 to get adequate resolution and reliable results.

5. Job Script Submission

After selecting the desired run script the user is prompted for the name of the subdirectory in which IRTOOL will store the outputs. It is convenient to enter the outputs of

each run into a different subdirectory. At this point the first option is to submit the current job script, which contains one run script corresponding to the current input parameters. The driver then runs the required modules in the correct sequence. The second option is not to submit the set of calculations, but go back, edit the input parameters and then write a second run script to the current job script buffer. In that case the driver does not start running the calculations and the first set of input parameters and desired calculations are stored in memory. There is no limitation on the number of scripts the user can write. The scripts are submitted by selecting the Submit job script command under the Run menu. The submitted jobs run in the background and as soon as they are complete a message is displayed in the IRTOOL window. In this case the run scripts are submitted all together and executed in the same sequence in which they were selected by the user. If we submit multiple job scripts they will run in parallel competing for computer resources [Ref.14].

The status of each job can be monitored from the Check Job Status command under the run menu. This command reports all the calculations which were submitted or which have been completed by the program. We can check also the output results subdirectory for the existence of error files (extension ".err"). If there is an empty error file either a module is still running or some errors have occurred during the calculations execution. If there is no error file then the program has completed the running of the job script without any error.

The Output menu provides commands which, when selected after the job finishes, launch IDL routines to display and analyze the line plot and image data files. The Create Inputs Text File command under the Output menu composes a text file including every input

parameter stored in memory. A detailed description of each module output can be seen by selecting the Module Outputs option under the Help menu.

The Toolbox menu contains interactive programs useful for constructing inputs needed by IRTOOL or for analysis of IRTOOL results [Ref.14]. The commands under the toolbox menu launch mainly IDL subroutines which execute various calculations such as calculating the solar position, editing the atmospheric profile generated by the atmosphere profiler module, etc.

The Help menu provides information about IRTOOL and its components, a tutorial, and some examples of how to use most of its features.

We must note here that after exiting IRTOOL the scripts that are still running, Toolbox applications and IDL routines launched from the Outputs or Toolbox menu that are still open, continue to run.

C. USER MODULE

Using a user module the user can increase the effectiveness and functionality of IRTOOL by developing and adding his/her own algorithms which will operate almost identically to the IRTOOL modules. The user module must be written in FORTRAN, IDL or in another programming language which can call FORTRAN. The user creates a user dialogue then generates the interface between his module and IRTOOL. The IRTOOL distribution includes an IDL module functioning with IRTOOL, several user modules, and subroutines which provide an interface between the user module, coded in FORTRAN or another

programming language which can call FORTRAN, and IRTOOL. After the user has compiled, linked and tested the code he/she can run the created executable code using an advanced or any-order run script containing the user module. Multiple user modules in sequence can be run with the limitation of being in separate runs.

D. MODEL ALGORITHMS

The IRTOOL program requires the calculations of the atmospheric profile and the atmosphere effects module to conduct ray tracing.

The atmosphere profiler module uses Monin-Obukhov similarity theory to predict the wind speed, temperature and humidity profiles in the marine boundary layer. The model parameters are air temperature, sea temperature, relative humidity, wind speed and relative height where the previous parameters were measured. The generated vertical profiles of temperature, wind speed, and water vapour content are logarithmic profiles. As we mentioned in section 2.B the bending of the ray is determined by the temperature gradient. This gradient is given by the following formula [Ref.15]

$$\frac{dT}{dz} = \frac{T_*}{a k z} \quad (15)$$

where T_* is a temperature scaling parameter

a is the heat transfer to momentum transfer ratio

k is the von Karman constant and

z is the height above sea surface.

The L(W)WKD and PIRAM marine boundary layer models are also based on Monin-Obukhov similarity theory and create atmospheric exponential profiles.

The atmosphere effects module of IRTOOL is responsible for the ray tracing in the marine boundary layer. Unlike the previous versions of the IRTOOL program, the latest version calculates the magnification effects of refraction using the continuous refractive index gradient profile created by the atmosphere profiler module. This model assumes that the Earth may be represented by a sphere, the atmosphere is a spherically stratified medium that is entirely characterized by the function $n(r)$, n being the refractive index at a point and r the distance of that point from the center of the sphere [Ref.16]. Taking into consideration these assumptions Snell's law for spherically symmetric geometry can be written [Ref.16]:

$$\frac{d}{ds}(n r \cos \beta) = 0 \quad (16)$$

where n is the index of refraction,

r is the distance from the earth's center

β is the ray angle with respect to the local horizon and

s the path length measured along the ray.

The program executes the calculations using the differential form of the previous relation [Ref.4]:

$$\tan \beta = \frac{d \ln r}{d\theta} \quad (17)$$

where θ is the earth centered angle through which the ray has propagated. Relation (17) following (16) becomes:

$$d\beta = \frac{d\theta}{n} \left(r \frac{dn}{dr} + n \right) \quad (18)$$

The combination of (16) and (17) is integrated using the Runge-Kutta method [Ref.17], to produce the equation of the ray in the form $r(\theta, \beta_0)$ where β_0 is the value of β for that ray when $\theta = 0$.

The L(W)WKD and PIRAM marine boundary layer models are used to provide profiles for application in combination with different ray tracing programs. These ray-trace programs were compared once in September 1996 and no significant differences were observed [Ref.15]. Therefore any deviation between their results is due to the L(W)WKD and PIRAM models and not to their different ray tracing programs.

IV. EXPERIMENTAL ARRANGEMENT AND PROCEDURE

A. INTRODUCTION

The Marine Aerosol Properties and Thermal Imager Performance (MAPTIP) experiment was carried out off the north coast of The Netherlands from October through November of 1993. The purpose of the experiment was to study the concentrations and properties of the marine aerosols and the performance of imaging systems in the marine boundary layer[Ref.12]. The experiment was organized under the NATO Research Specialty Groups on boundary layer composition and imaging systems, and was executed by a multinational group of researchers from the United States, Canada, France, Germany, The Netherlands, United Kingdom, Norway and Denmark, and delivered a great amount of refraction and atmospheric characterisation measurements. The refraction data used in this analysis were provided by DREV, CA., and CELAR, FR., with supporting characterisation data from other members of the MAPTIP group.

B. EXPERIMENTAL SETUP

Throughout the MAPTIP experiment two experimental techniques for refraction measurements were used, both developed by DREV, Canada. During the first one, a number of visible/IR sources are placed at fixed heights and fixed distances from an observation station where a series of visible and IR sensors are placed at various heights. This technique is used to correlate the observed relative angles between the sources and the ones predicted

by the models that are to be compared. During the second technique a series of visible and IR radiation sources are placed at various heights on a ship which moves away from the same observation station used for the first technique. The purpose of this technique is to observe and report the Minimum Mirage Ranges in the cases that mirage occurs, and the Maximum Inter-vision Ranges of the ship's sources. The data sets provided to be analysed in this thesis were extracted from the measurements using the second technique during the ship observations.

Hr. Ms. Tydeman was the Dutch navy research ship that participated in this experiment. The radiation sources placed on Tydeman were six (500W) halogen lamps mounted at various heights on the stern of the ship as shown in Figure 6. The source heights used were 3.34, 6.38, 11, 11.45, 14.5 and 20.7m above the water level. The ship was ordered to move in a straight course away from the shoreline while it was tracked by a series of visible and IR cameras located in a beach station. The cameras were placed at various heights above the Mean Water Level as shown in Figure 7. Their types and characteristics are summarized in Table 1.

The data sets obtained during the experiment were the video recordings of the Tydeman moving away from the beach, referred as ship tracking events [Ref. 12]. Thirteen ship tracking events were conducted. For convenience, these are labeled A to M. The recorded values for each event of the meteorological data, sea temperature, air temperature, relative humidity, air pressure, wind speed and direction, water level with respect to MWL (tide height), $H_{1/3}$ wave height, solar radiation, rain rate and air sea temperature difference (ASTD) are summarized in Table 2.

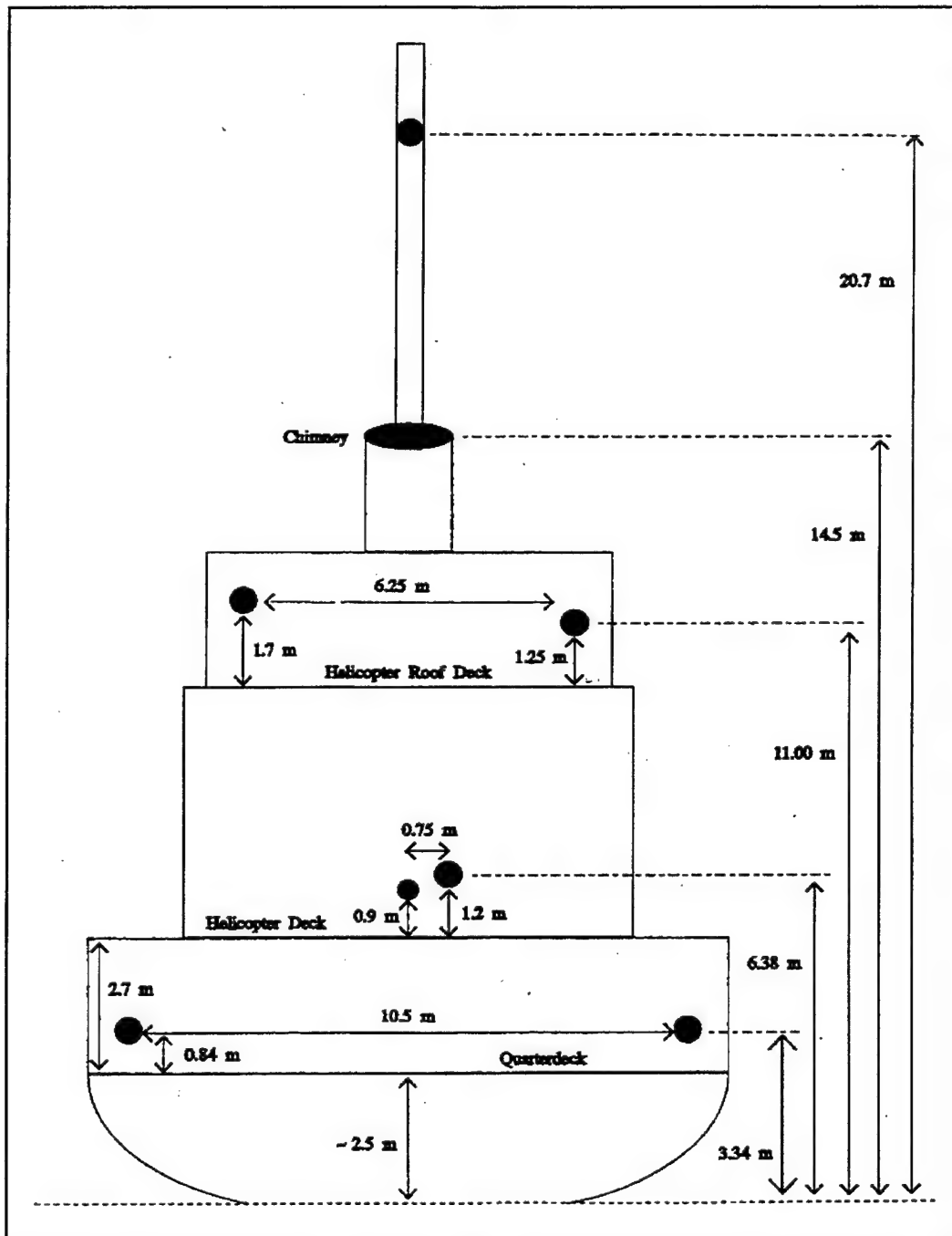


Figure 6. Schematic diagram of the Hr. Ms. Tydeman with the placement of the six halogen lamps, the exhaust stack, and the stern light 0.9 m above the helicopter deck (100W). [From Ref.12]

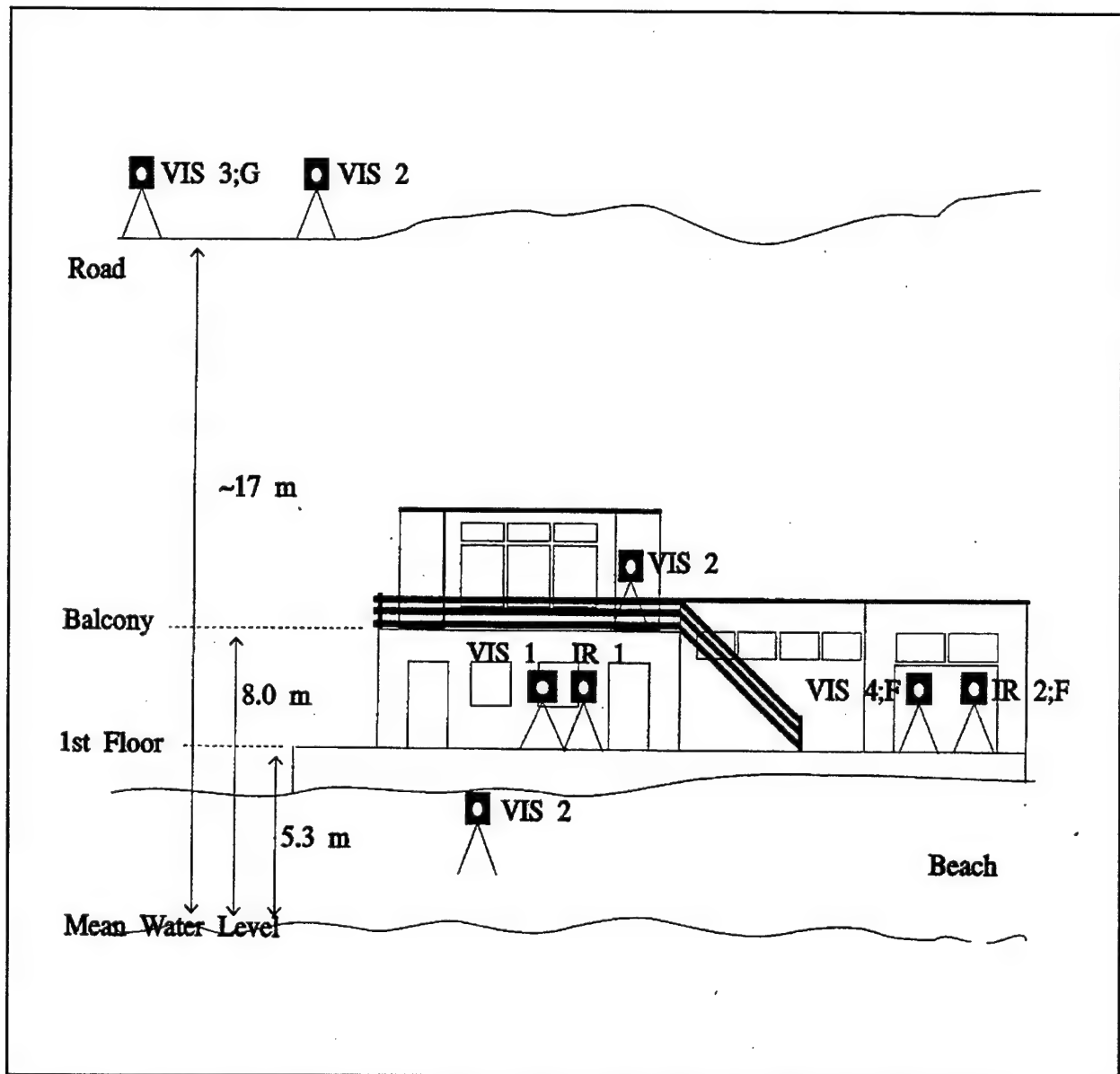


Figure 7. Schematic diagram of the beach station showing the location of the various cameras used during the MAPTIP trial [From Ref.12].

Camera	Country	Type	Wavelength (μm)	Resolution ($\mu\text{rad/pixel}$)
V1	Canada	Sony CCD	> 0.85	$6.23 \pm 2\%$
V2	Canada	Sony CCD	> 0.715	$9.15 \pm 2\%$
V3	Germany	CCD	visible	$11.94 \pm 2\%$
V4	France	Sony CCD	visible	$161 \pm 5\%$
IR1	Canada	Mitsubishi	3-5	$9.91 \pm 2\%$
IR2	France	Castor	8-12	$139 \pm 5\%$
IR3	France	Mitsubishi	3-5	$468 \pm 5\%$

Table 1. Characteristics of the visible and Infrared cameras used during the MAPTIP experiment [After Ref.2].

Weather Summary used for the Tydemann Measurements													
Parameters	A	B	C	D	E	F	G	H	I	J	K	L	M
Date (dd-mm-yy)	10/19/93	10/20/93	10/21/93	10/22/93	10/22/93	10/25/93	10/25/93	10/26/93	10/27/93	10/27/93	10/28/93	10/29/93	10/29/93
Start (hh:mm)	8:25	7:25	8:05	14:45	20:45	3:35	15:40	8:35	7:35	12:45	8:35	14:30	21:10
Stop (hh:mm)	9:20	8:25	9:05	15:40	21:55	4:40	16:25	9:45	8:20	13:35	9:35	15:30	22:00
Water Temp. (C)	13.60	12.50	12.70	12.40	12.40	11.60	11.50	11.50	11.60	11.70	11.70	11.50	11.40
Ht. of Sensor 1 (m)	15.00	12.00	3.40	3.40	3.40	3.40	3.40	3.40	3.40	3.40	3.40	3.40	3.40
Air Temp. (C)	4.10	8.40	8.30	9.10	7.40	11.00	10.30	11.20	9.90	10.30	9.20	9.00	6.30
Rel. Humidity (%)	80.00	65.00	80.00	72.00	76.00	73.00	77.00	85.00	86.00	85.00	80.00	80.00	87.00
Air Pressure (mbar)	1033.0	1026.0	1011.0	1025.0	1027.0	1030.0	1031.0	1031.0	1030.0	1028.0	1027.0	1025.0	1027.0
Ht. of Sensor 2 (m)	27.4	22.6	3.4	3.4	3.4	3.4	3.4	3.4	3.4	3.4	3.4	3.4	3.4
Wind Speed (m/s)	5.0	5.0	9.5	9.8	9.1	7.3	8.2	7.0	5.1	4.4	4.1	5.1	5.7
Wind Direction (deg)	90.0	280.0	345.0	50.0	60.0	25.0	30.0	40.0	40.0	35.0	82.0	75.0	90.0
Water Level (m)	-0.4	0.3	0.9	-1.0	0.3	-0.5	-0.8	-0.6	-0.7	0.6	-0.8	0.5	-1.0
Wave Height (m)	0.3	0.2	1.9	1.0	0.9	0.9	0.9	0.7	0.8	0.7	0.5	0.4	0.4
Solar Radiation (W/m2)	300.0	70.0	35.0	30.0	0.0	0.0	5.0	140.0	30.0	125.0	75.0	120.0	0.0
Rain Rate (mm/10 min)	0.0	0.0	0.1	0.0	0.0	0.0	0.0	0.0	0.0	0.0	0.0	0.0	0.0
ASTD (C)	-9.5	-4.1	-4.4	-3.3	-5.0	-0.6	-1.2	-0.3	-1.7	-1.4	-2.5	-2.5	-5.1

Table 2. Summary of the meteorological data during the MAPTIP experiment [After Ref.13]

V. DATA ANALYSIS

A. INTRODUCTION

As mentioned in the previous chapters the factor that most affects the refractivity profile in the lower part of the Marine Boundary Layer (MBL) is the temperature profile. The IRTOOL program as well as LWKD and PIRAM are used for the prediction of the optical/IR ray behavior in the MBL. In Chapter III we presented IRTOOL, as used in this thesis, as a combination of an atmospheric profiler and a ray tracing program. However the LWKD and PIRAM programs are MBL models which create the atmospheric profile and then are used with other ray tracing programs to generate the desired calculations.

In that chapter we examine the IRTOOL capability to produce mirage effects. Another MBL program used as an alternative for the atmosphere profiler module will be briefly presented. The MMRs and MIVRs for various atmospheric conditions, passbands, target positions and sensor positions as calculated by IRTOOL, LWKD and PIRAM, are also compared with the experimental data recorded during the MAPTIP experiment. Finally, we discuss the reasons for possible deviation between the results of the programs and the experimental data; techniques to improve the results of the programs and accomplish the closest possible fit to the experimental data are also given.

The required IRTOOL calculations for the analysis were produced in this work using Version 2.1 of the IRTOOL program, which is installed in the simulation lab of the Physics Department of the Naval Postgraduate School (NPS). The predictions of the other models

were calculated in 1995 and 1996 so any recent changes of the models are not reflected in this comparison.

For the extraction of the required results we ran the Default Run Script of Engagement, Atmosphere and Ray Refraction. The modules used for the calculations were the atmosphere profiler, the atmosphere effects without radiance, and the engagement module. The inputs inserted in the program for each run are shown in Table 3. The required inputs for each parameter group of the program are many more, but we can leave the defaults for these inputs as they are used for other run scripts which enable additional modules, and in our case do not affect the final result. The needed IRTOOL MIVRs and MMRs were taken using the Plot Curves command under the Output menu. Using the launched IDL routine we opened the “atm_engage_b01.plt” file generated by each run into the output subdirectory, and displayed all the desired data.

Group type	Parameters
Sensor	Passband- Lambda Min Passband- Lambda Max
Sensor operation	Sensor altitude
Environment-atmosphere	Reference height Air temperature at h0 Relative humidity Wind speed at h0 Sea temperature
Target-trajectory	Target range max Target range min Target altitude Output control

Table 3. IRTOOL parameters needed for the calculations

B. NPS ATMOSPHERE PROFILER

As a comparison to the IRTOOL generated atmospheric profile, and to use IRTOOL only as a ray tracing program, we operated, as an alternative to the atmosphere profiler module, a MBL program created by the Boundary Layer Studies Group of the Meteorology Department of the Naval Postgraduate School. This computer program, provided by Prof. K. Davidson of the Meteorology Department, is written in MATLAB programming language. For simplicity reasons we will refer to it as "NPS atmosphere profiler."

The NPS atmosphere profiler requires some meteorological parameters to produce the profile of air temperature, specific humidity, modified refractivity (for wavelengths greater than 3mm) and atmospheric pressure. As for all previous programs, it uses Monin Obukhof Similarity Theory to create the desired profiles. We made a slight modification to the program in order for each run to produce only the air temperature profile and a matrix of the heights in fractions of 0.1 m, and the corresponding air temperatures. This matrix will be used in the atmosphere shaper to create a custom profile. Then using the advanced flow control we will run IRTOOL operating only its ray tracing features.

The meteorological data required by the NPS atmosphere profiler are air temperature, relative humidity, wind speed, sea temperature and atmospheric pressure. The significant difference between the NPS atmosphere profiler and the IRTOOL profiler is that the user of the NPS atmosphere profiler must input the reference height for each meteorological data input while IRTOOL requires only one reference height, assuming that all data were measured at that height.

Trying to correlate the above programs, we ran them several times. Figures 8 and 9 show plots of the air temperature profiles of ship tracking events B and K (see Table 2) which are results of the comparison between the above models for negative air to sea temperature differences (ASTD= - 4.1°C and ASTD= - 2.5°C) while Figures 10 and 11 are hypothetical examples that correspond to positive ones (ASTD =1.0°C and ASTD = 2.0°C). It is obvious that the two programs create temperature profiles that match perfectly when ASTD is negative and differ only slightly for heights above 30m when ASTD is positive. Because the region of the MBL that most affects the behavior of the optical/IR rays is the first few meters above the surface and additionally, because the ASTD's in the provided data are always negative, for the purpose of analysis we will consider the temperature profiles generated by the two models identical.

C. DATA ANALYSIS

The data which were analyzed were provided by Dr. L. Forand of DREV, coordinator of the "Refractive effects in the visible and the IR" work group, which was responsible for analyzing and combining the results of the various MAPTIP refraction measurements.

The plots produced for the analysis include the recorded MMRs and MIVRs during the MAPTIP experiment and the calculations of the LWKD and PIRAM models as well as the calculations of IRTOOL. In each plot created we used the same symbols to represent calculations of the same model. The right-most solid line with the solid rhombus ('◆')

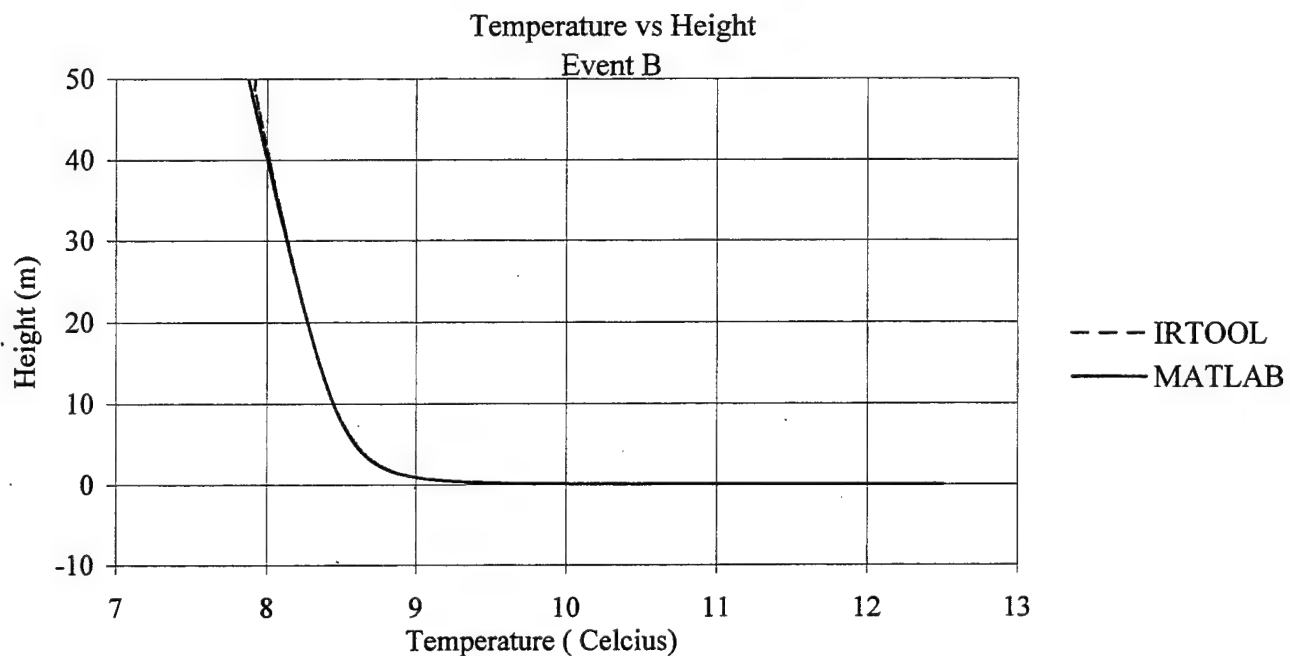


Figure 8. Comparison between the IRTOOL profiler and the NPS atmosphere profiler for negative air to sea temperature differences (ASTD=-4.1)

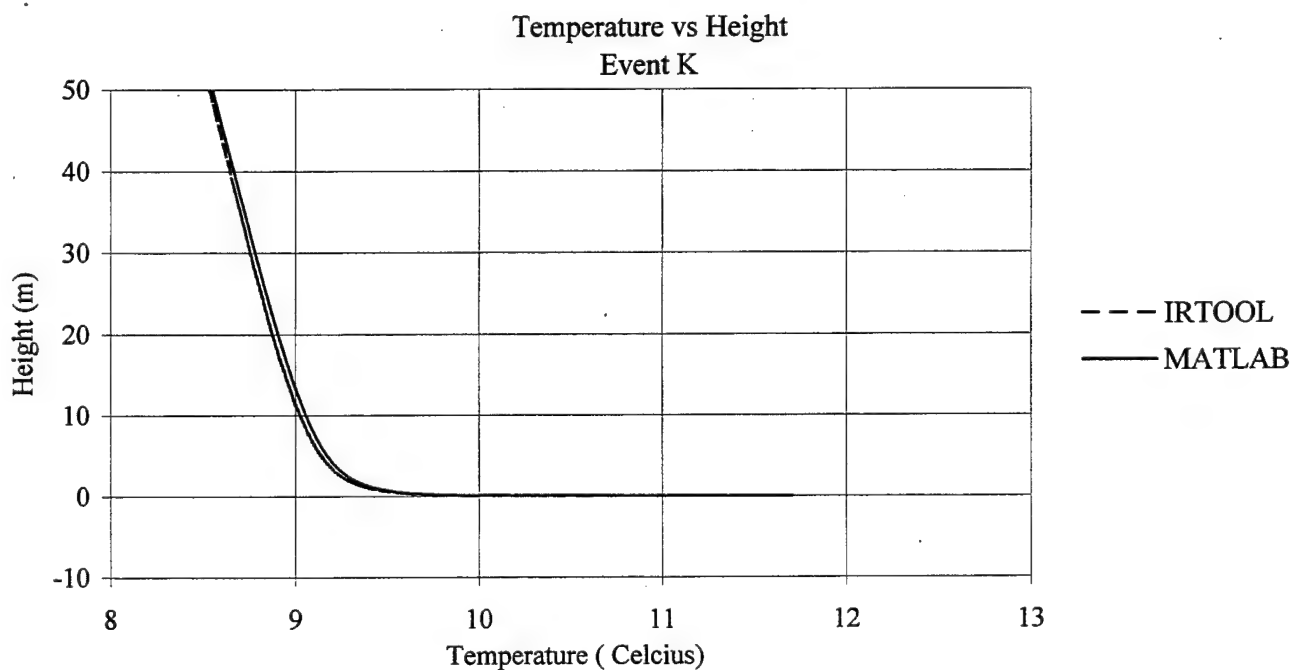


Figure 9. Comparison between the IRTOOL profiler and the NPS atmosphere profiler for negative air to sea temperature differences (ASTD=-2.5)

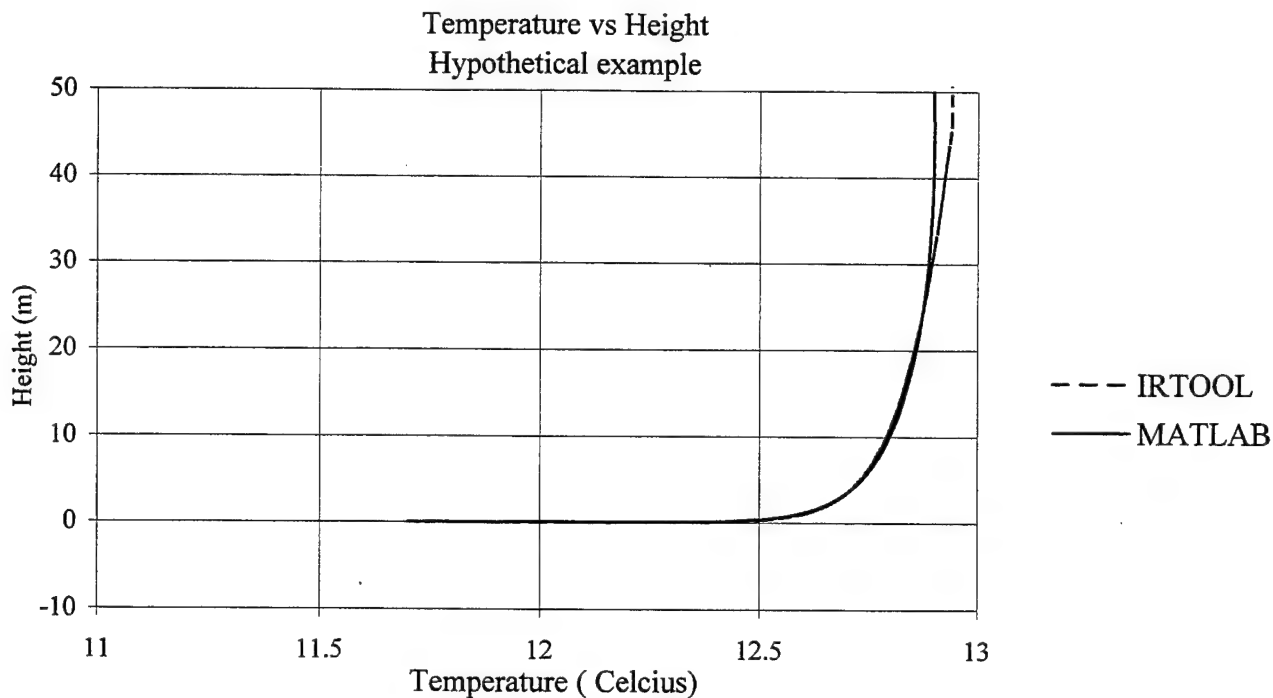


Figure 10. Comparison between the IRTOOL profiler and the NPS atmosphere profiler for positive air to sea temperature differences (ASTD=1.0)

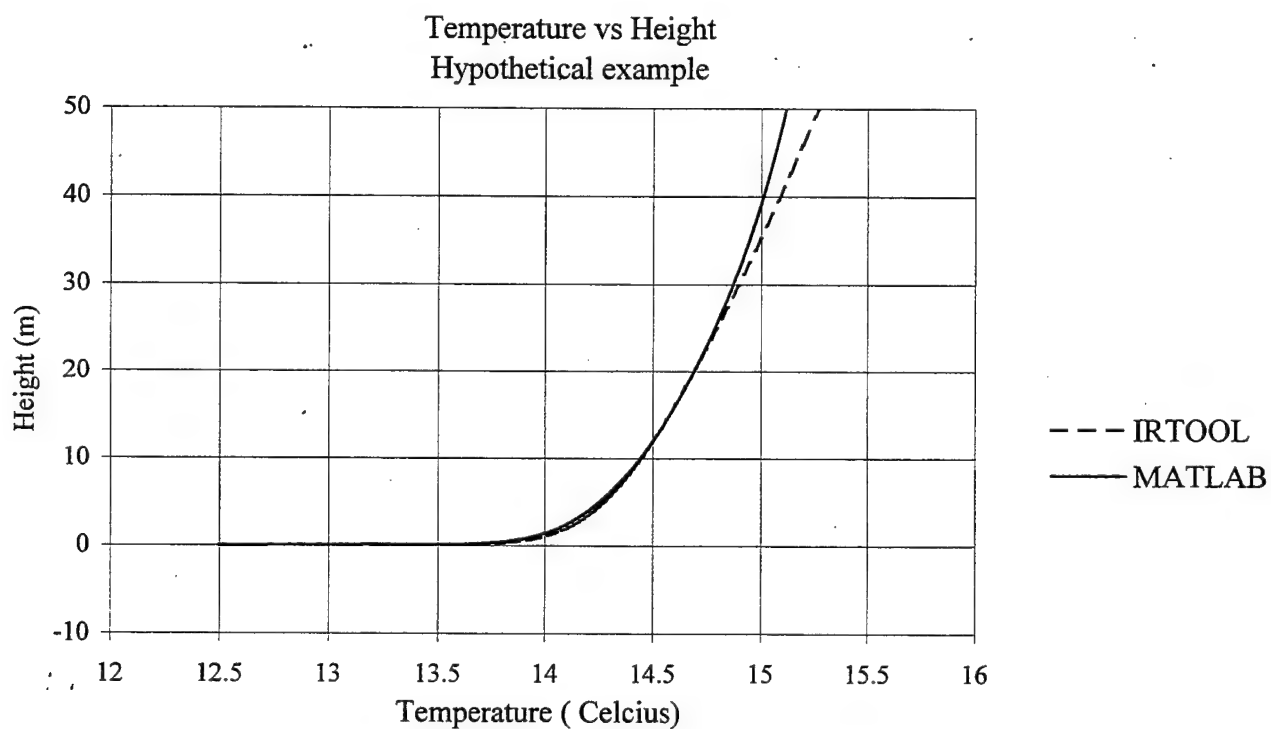


Figure 11. Comparison between the IRTOOL profiler and the NPS atmosphere profiler for positive air to sea temperature differences (ASTD=2.0)

represents the geometrical horizon or else the maximum inter-vision range for a non refractive atmosphere. The triangles ('▲') represent the observed experimental data for the Maximum Inter-Vision Range or the Minimum Mirage Range in accordance with what the plot shows, while the solid line that connects these points is a 2nd order polynomial fit. The circles ('●'), squares ('■') and x's ('X') represent results of IRTOOL, PIRAM and LWKD model calculations respectively, for each one of the lights/targets on the ship. All the reported sensor heights (h_s) are measured from the water level.

1. Ship Tracking Event B

Figure 12 shows the results of the model comparison for MIVR data observed by the V2 visible camera ($h_s=5.8$ m) during ship tracking event B. As we can see from these curves all models predict similar MIVRs that are always shorter than those from the experimental data. The LWKD model results are ~2 km shorter, the PIRAM results are 2-2.5 km shorter and the IRTOOL results 2.5-3 km shorter. Figure 13 shows the results of the corresponding model calculations for the minimum ranges at which mirage can be observed. The LWKD model results are almost coincident with the experimental data, the PIRAM results are 1 to 1.6 km shorter and the IRTOOL results are 1.4 to 4.5 km longer, the difference increasing with the elevation of the light/target.

Figures 14 and 15 show the results of the model comparison for the data observed by the IR1 (3-5 μ m) infrared camera ($h_s=6.23$ m). The LWKD model results for the MMR are 0.5 to 1.0 km shorter, the PIRAM results are 1.0 to 2.0 km shorter and the IRTOOL results

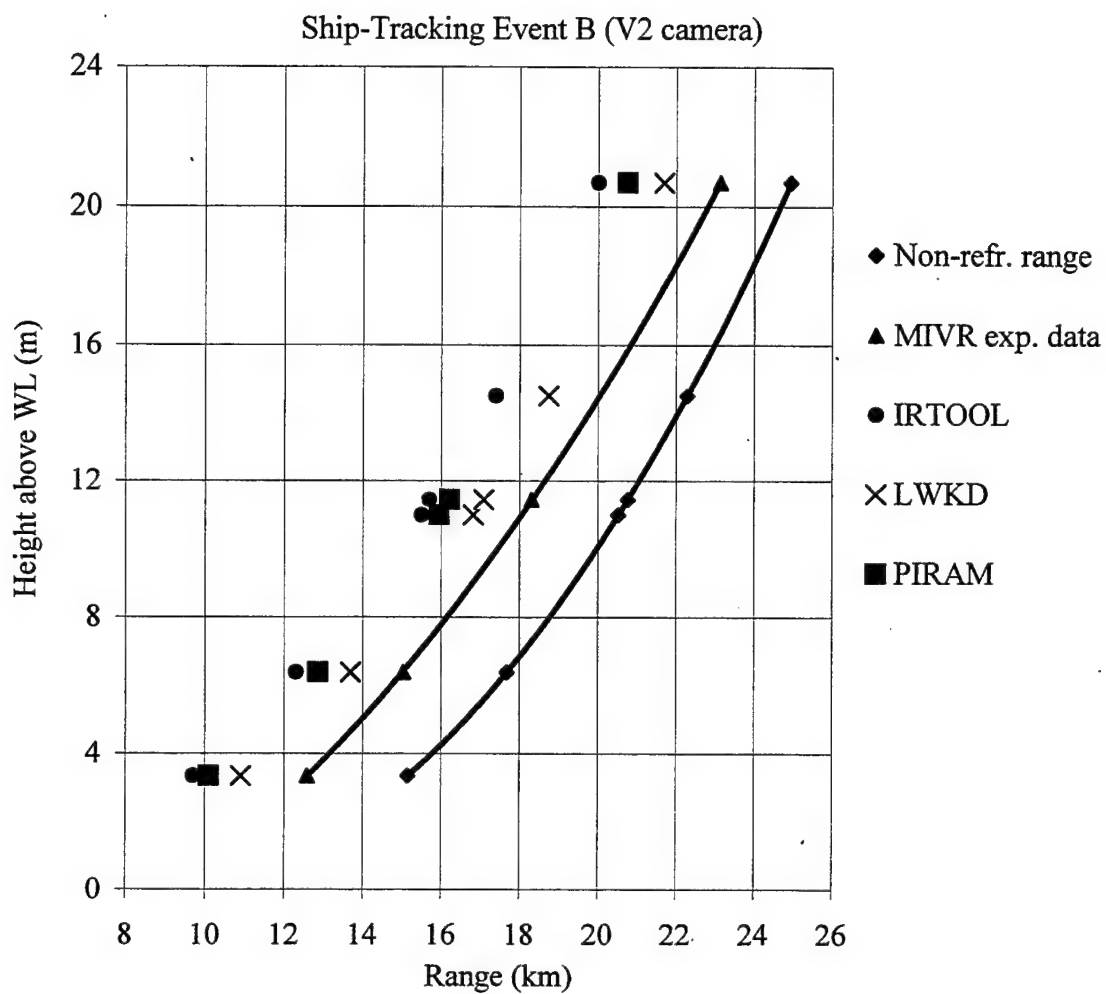


Figure 12. Comparison of the LWKD, PIRAM and IRTOOL model MIVRs with the ship-tracking data measured by the V2 visible camera

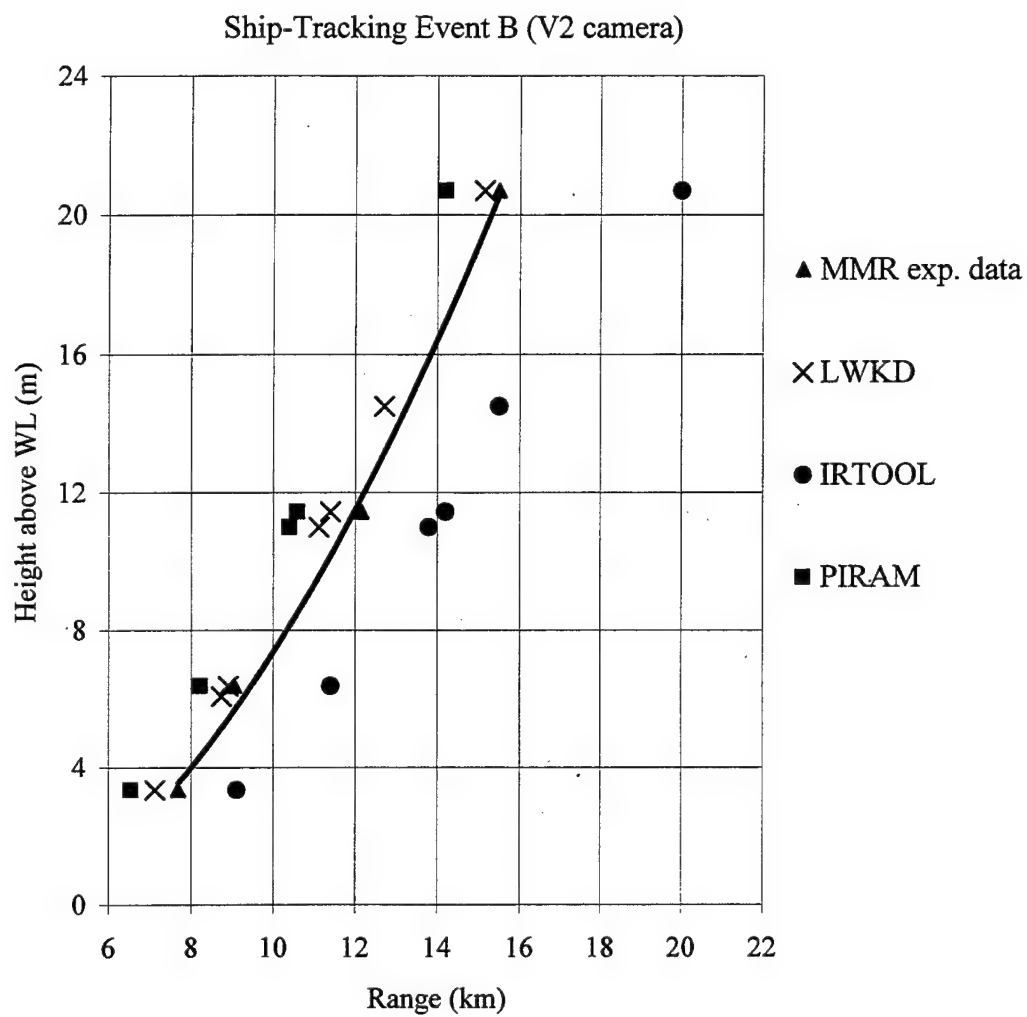


Figure 13. Comparison of the LWKD, PIRAM and IRTOOL model MMRs with the ship-tracking data, measured by the V2 visible camera

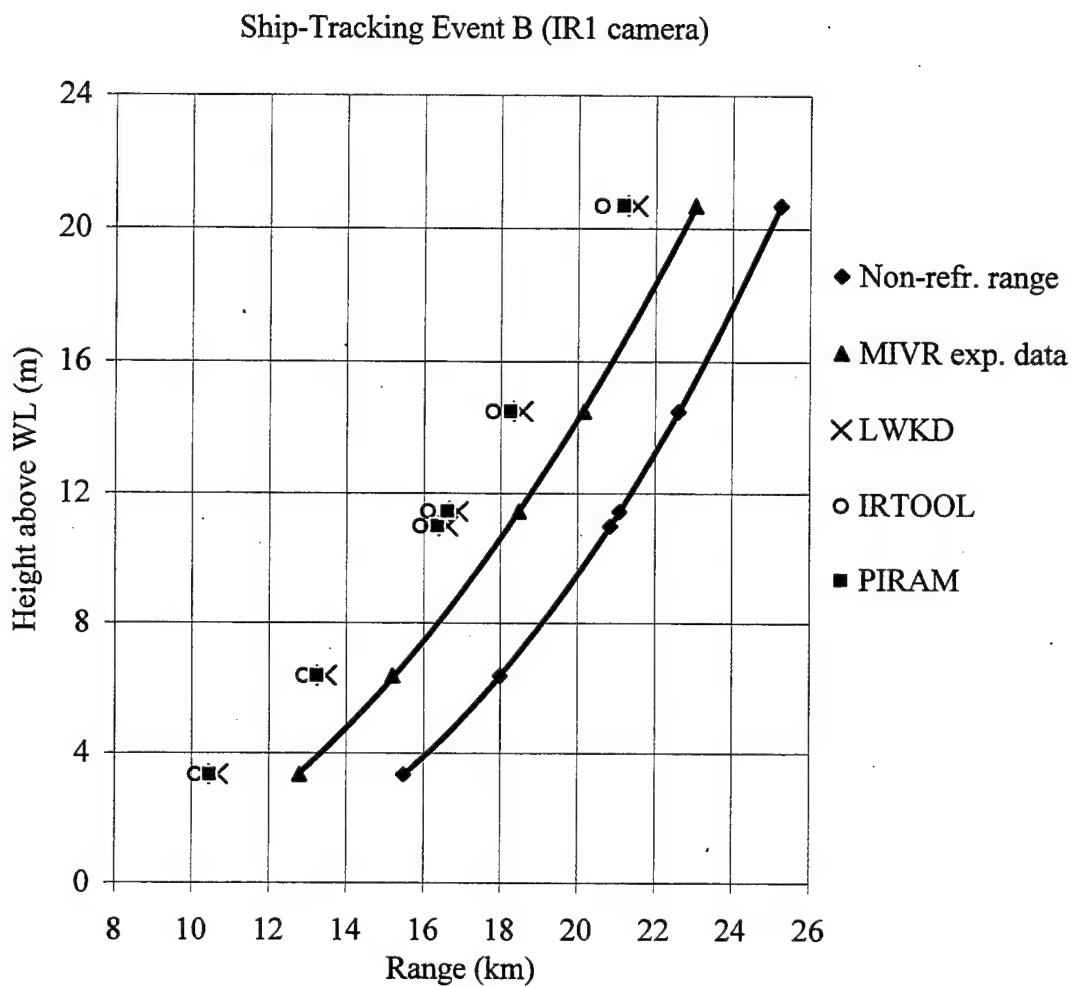


Figure 14. Comparison of the LWKD, PIRAM and IRTOOL model MIVRs with the ship-tracking data, measured by the IR1 (3-5 μ m) camera

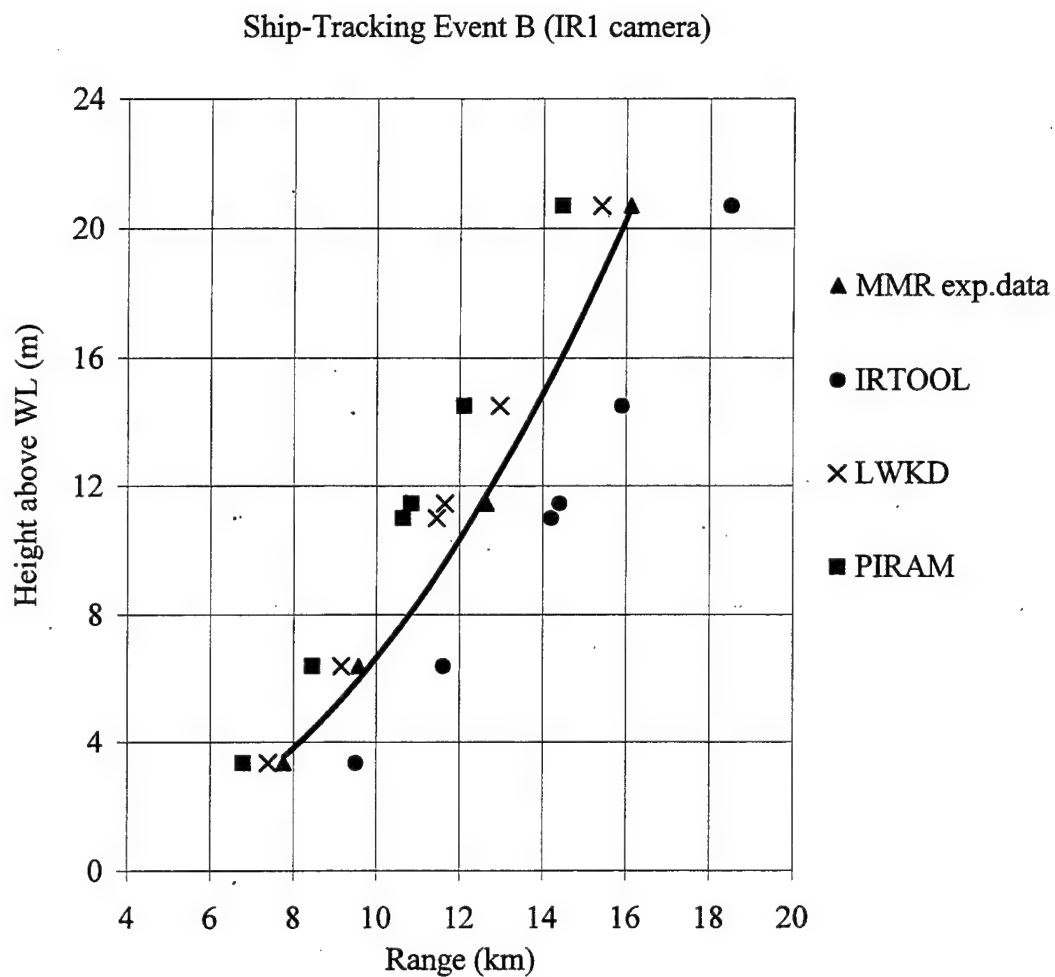


Figure 15. Comparison of the LWKD, PIRAM and IRTOOL model MMRs with the ship-tracking data, measured by the IR1 (3-5 μ m) camera

1.7 to 2.4 km longer. For the MIVR the LWKD model results are 1.5 to 2.2 km shorter, the PIRAM results are 1.9 to 2.4 km shorter and the IRTOOL results are 2.3 to 2.7 km shorter.

The difference between the observed data and the ones calculated by the models may be attributed to one or more of the following:

a. IRTOOL assumes that all meteorological data are measured at the same height, which was not the case during event B. The air temperature (T_a) and humidity (R_h) were measured at 12m while the anemometer is placed at a height of 22.6m. From the IRTOOL generated wind speed profile of Figure 16 we notice a difference of 0.15 m/sec between the wind speed values at 12 m and 22 m. That difference is insignificant as a reason for the deviation of results. This conclusion was verified by running the NPS atmosphere profiler and inserting the resulting temperature profile in IRTOOL, used as a ray tracing program. Again the results were not close to the experimental data.

b. The tolerances of the model input parameters. All the model results were calculated for the ASTD value of -4.1°C shown in the tabulation of Table 2. This is inconsistent with the shipboard measurements for the ship tracking event B. There is an ASTD variation of 2° along the course of the ship as is seen in Figure 17. The measuring equipment tolerances, the fact that the subsurface sea temperature gradient is very large and the depth of the measurement of the sea temperature isn't fixed increase the ASTD uncertainty.

The effects of this parameter change were considered by making a small modification of the meteorological data, taking $\text{ASTD} = -3.1^{\circ}\text{C}$ instead of the measured -4.1°C . This

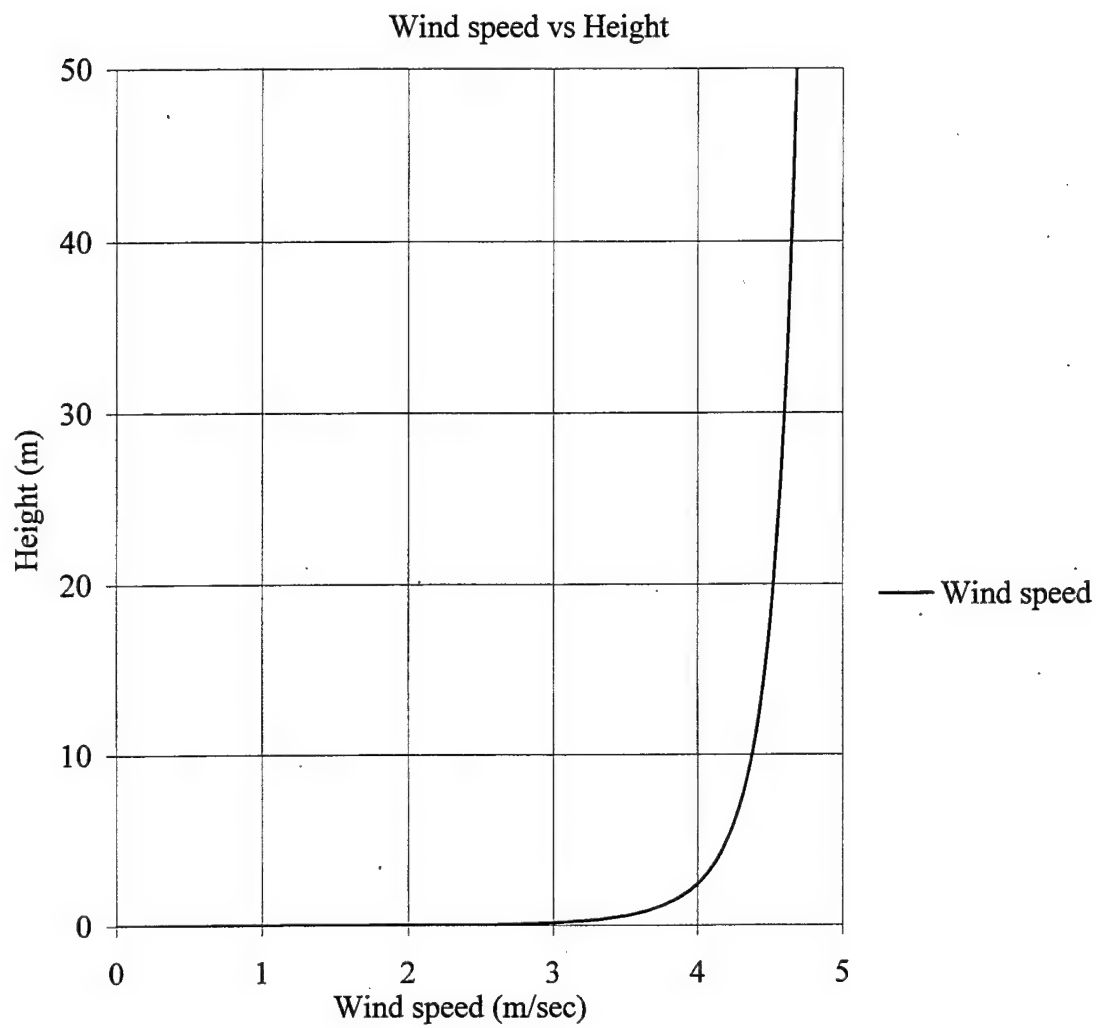


Figure 16. Wind speed profile generated by IRTOOL for the ship-tracking event K

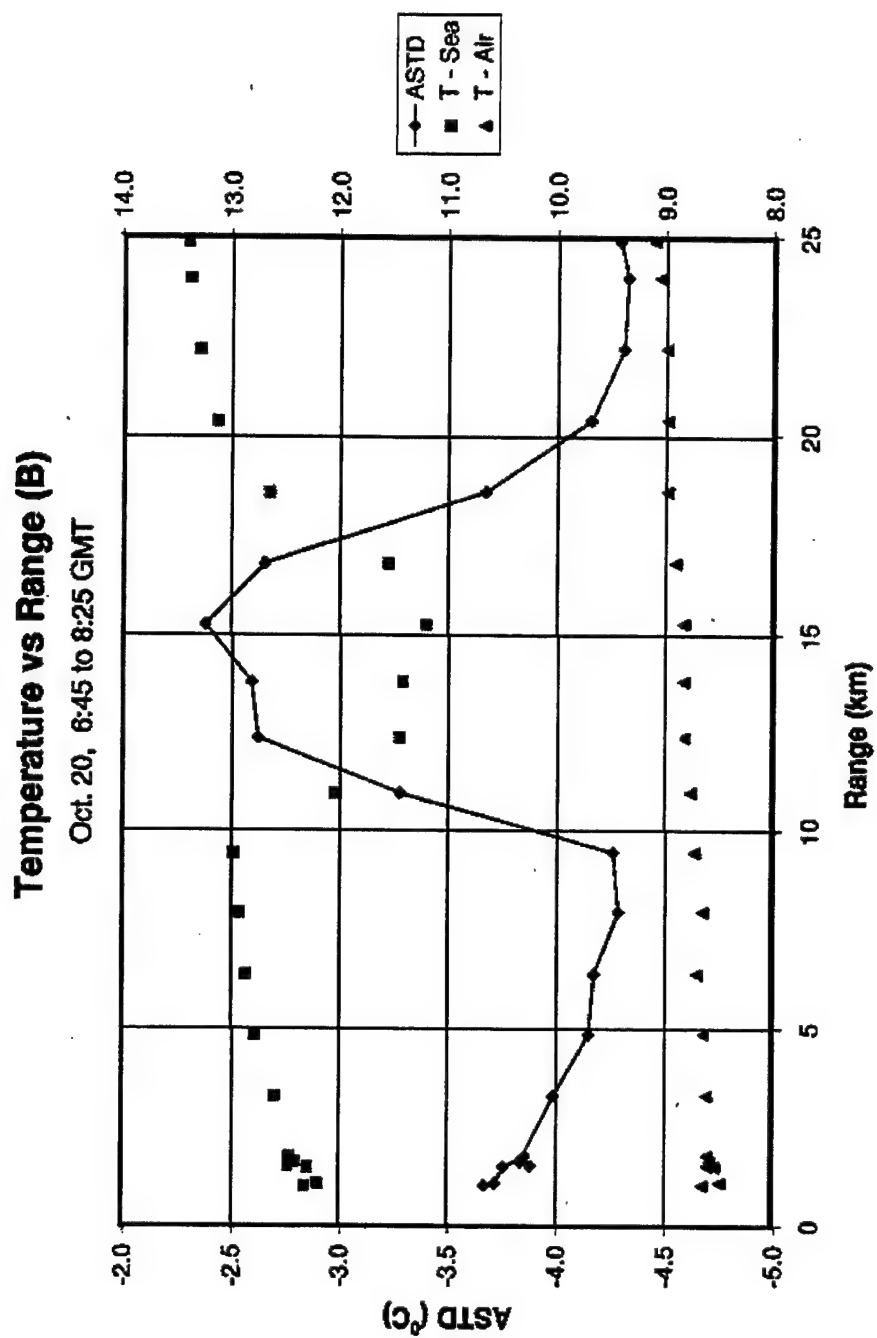


Figure 17. Variation of sea temperature along the ship's course during ship tracking event B

modification led to the corresponding LWKD and PIRAM calculations giving MIVR and MMR closer to the experimental data. Figures 18 to 19 show the comparison of IRTOOL's predictions for ASTDs -4.1°C , -3.1°C and -2.6°C . The predictions of the MIVR improve slightly while the MMR predictions move off the experimental data points.

2. Ship Tracking Event K

The next set of data was measured during the ship tracking event K during which the ship was tracked by the visible cameras V1 through V4 and the infrared cameras IR1 and IR2.

Figures 20 to 25 show the results of the models comparison for the data observed by the V1 ($h_s=8.62$ m), V2 ($h_s=5.43$ m) and V4 ($h_s=8.21$ m) visible cameras. The LWKD predicts MIVRs that are 0.5 to 1.4 km short of the experimental data, the PIRAM results are 1.0 to 2.0 km shorter, and the IRTOOL results are 0.9 to 1.8 km shorter. The MMRs predicted from LWKD match perfectly or they are within 1 km of the experimental data. PIRAM predicts MMRs that are 0.2 to 1.9 short of the experimental data. Finally the IRTOOL predicts ranges that are identical or they are within 0.8 km of the experimental data.

The results of the model comparison for the data observed by the IR1 ($h_s=8.62$ m) infrared camera are shown in Figures 26 and 27. The LWKD predicts MIVRs that are 0.4 to 1.3 km short of the experimental data, the PIRAM results are 1.1 to 1.8 km shorter, and the IRTOOL results are 1.0 to 1.7 km shorter. The MMRs predicted from LWKD match perfectly or they are within 0.6 km to the experimental data. PIRAM predicts MMRs that are

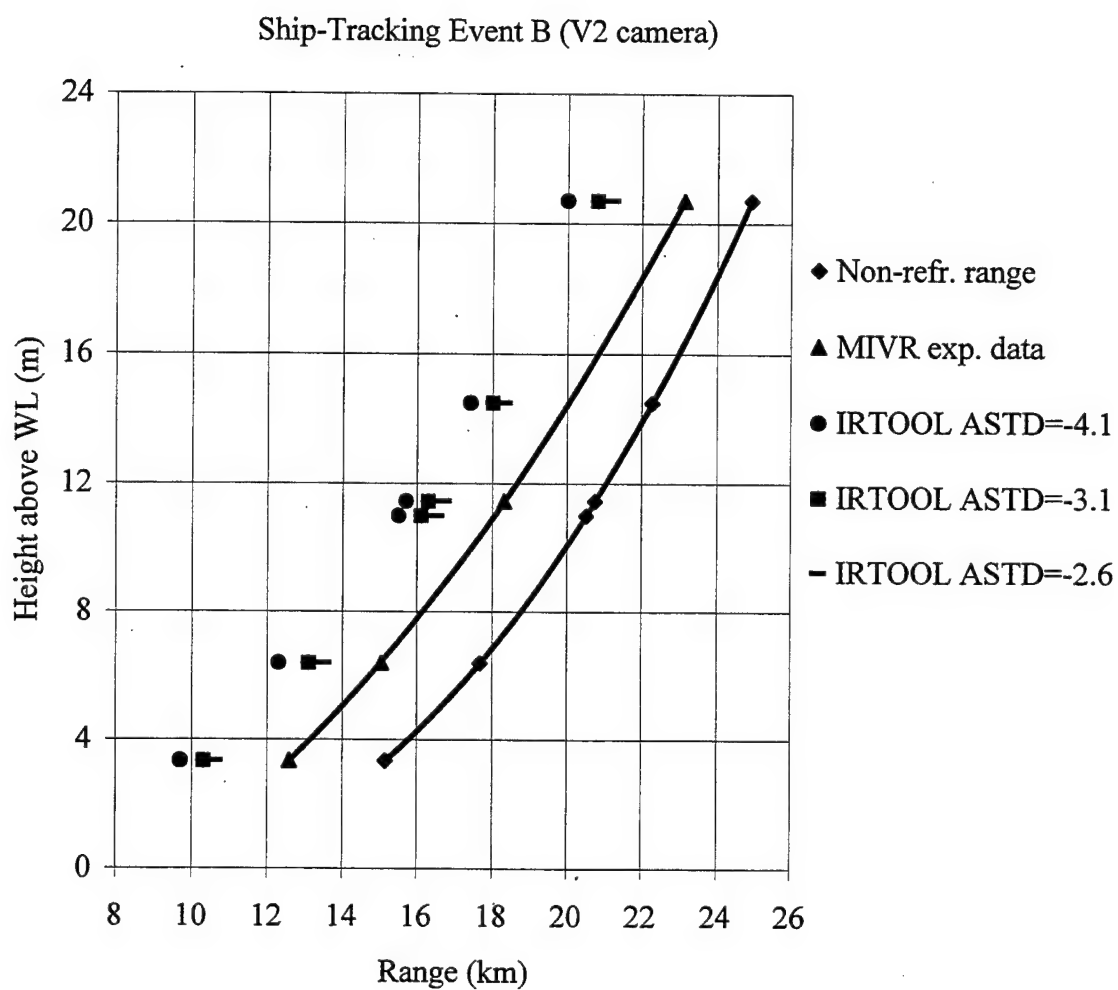


Figure 18. Comparison of the predictions of IRTOOL (MIVR) for ASTDs -4.1, -3.1 and -2.6°C with the ship-tracking data, measured by the visible camera

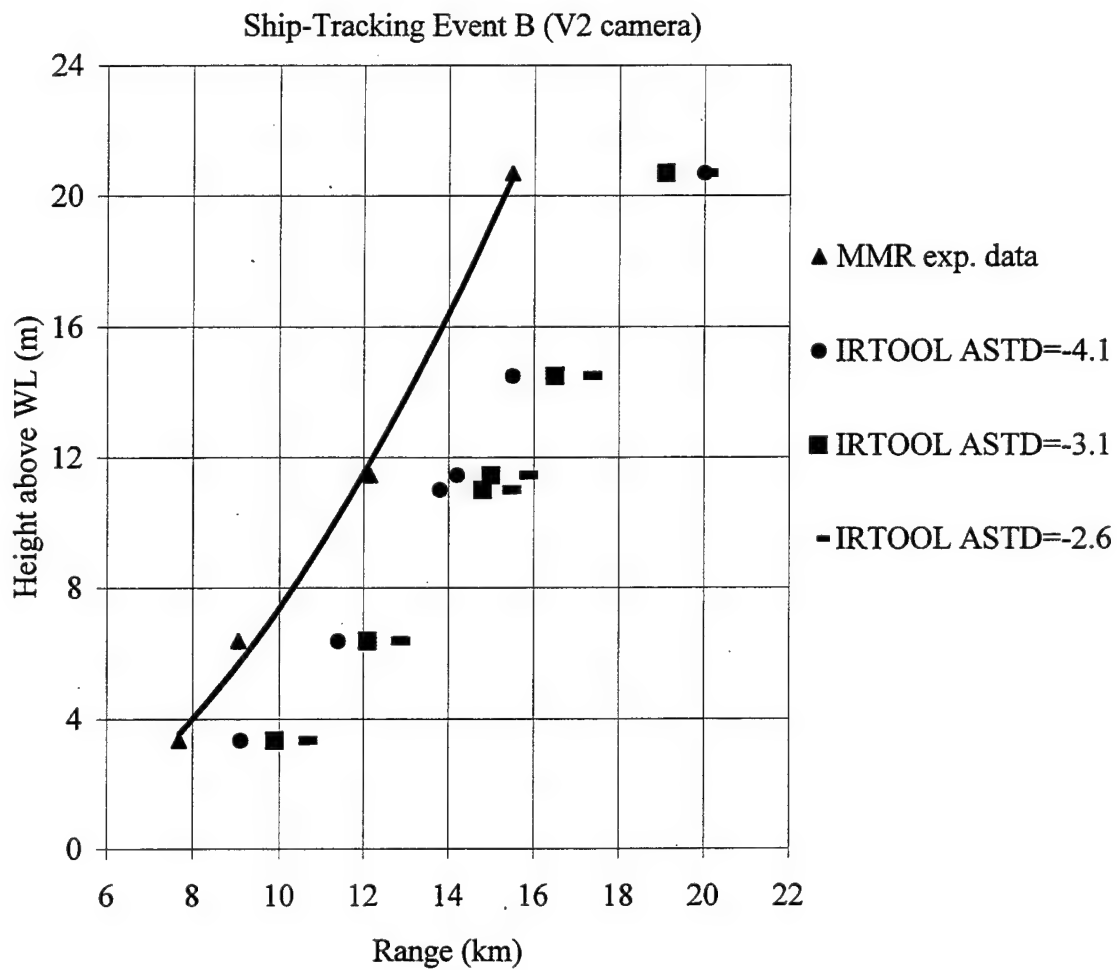


Figure 19. Comparison of the predictions of IRTOOL (MMR) for ASTDs -4.1, -3.1 and -2.6°C with the ship-tracking data, measured by the visible camera

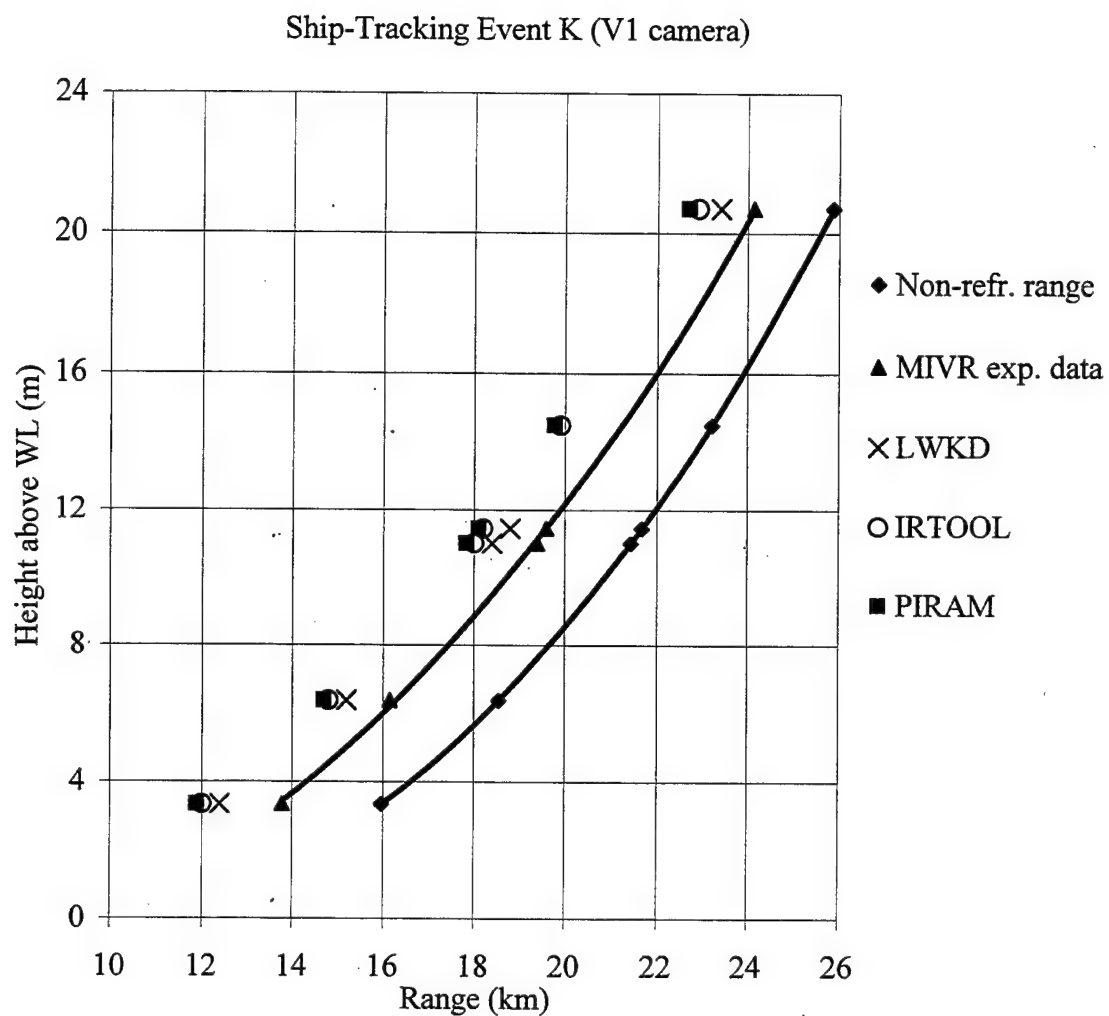


Figure 20. Comparison of the LWKD, PIRAM and IRTOOL model MIVRs with the ship-tracking data measured by the V1 visible camera

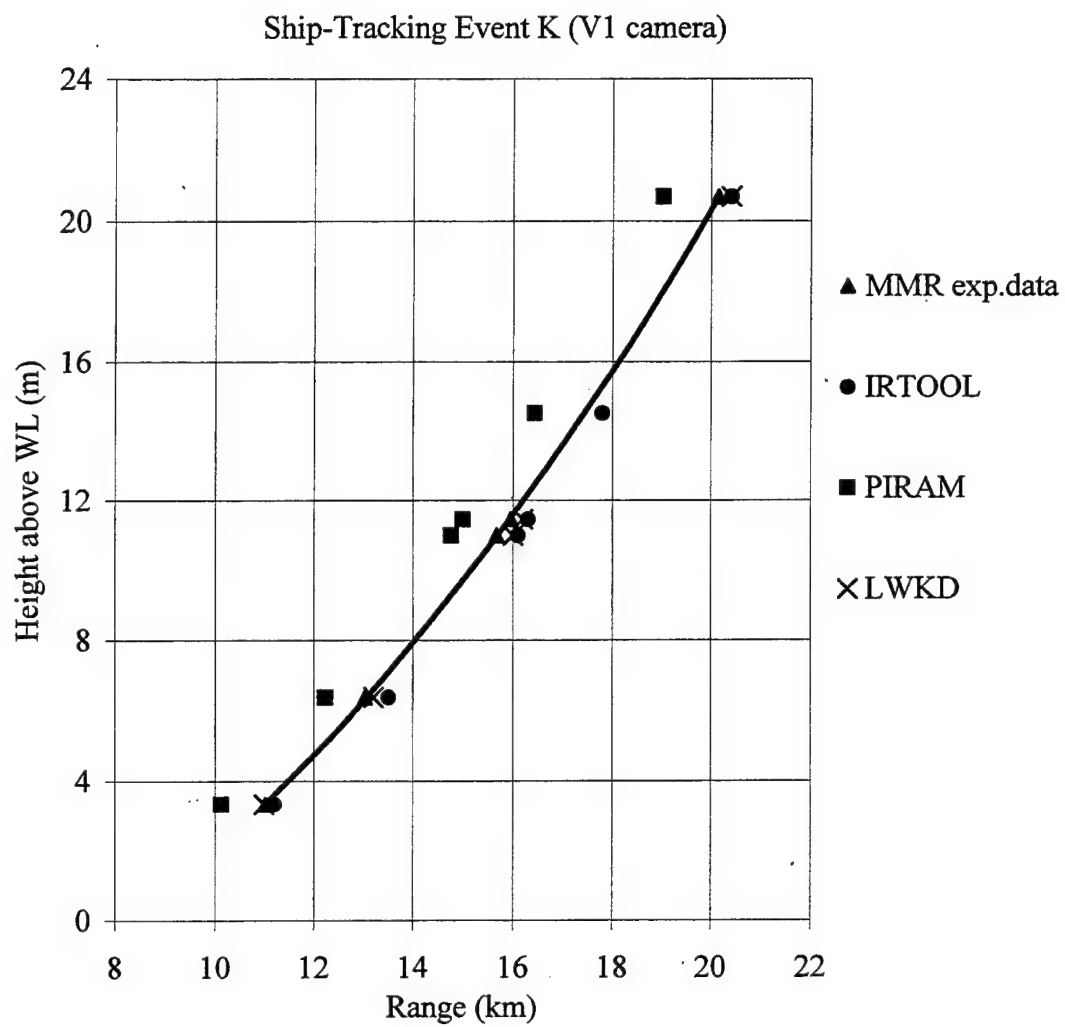


Figure 21. Comparison of the LWKD, PIRAM and IRTOOL model MMRs with the ship-tracking data measured by the V1 visible camera

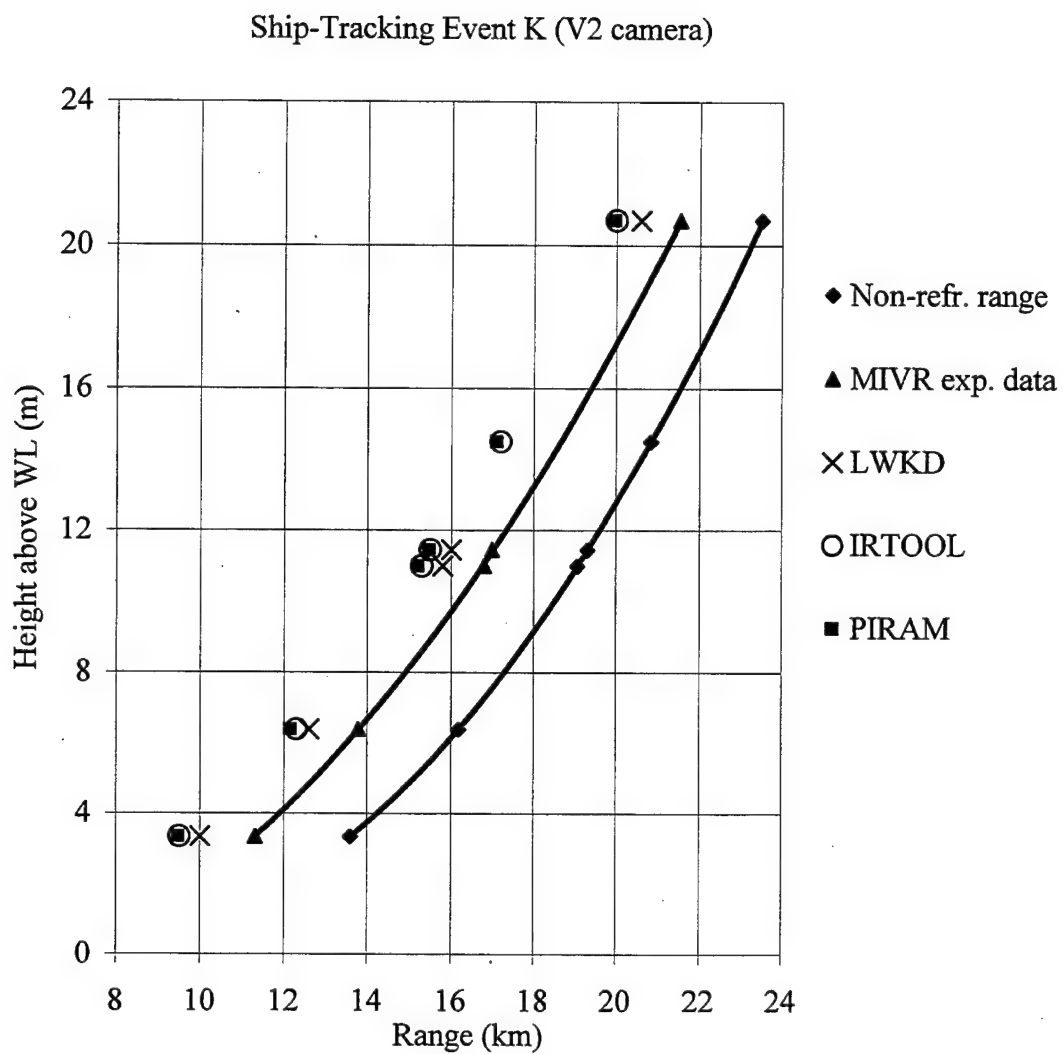


Figure 22. Comparison of the LWKD, PIRAM and IRTOOL model MIVRs with the ship-tracking data measured by the V2 visible camera

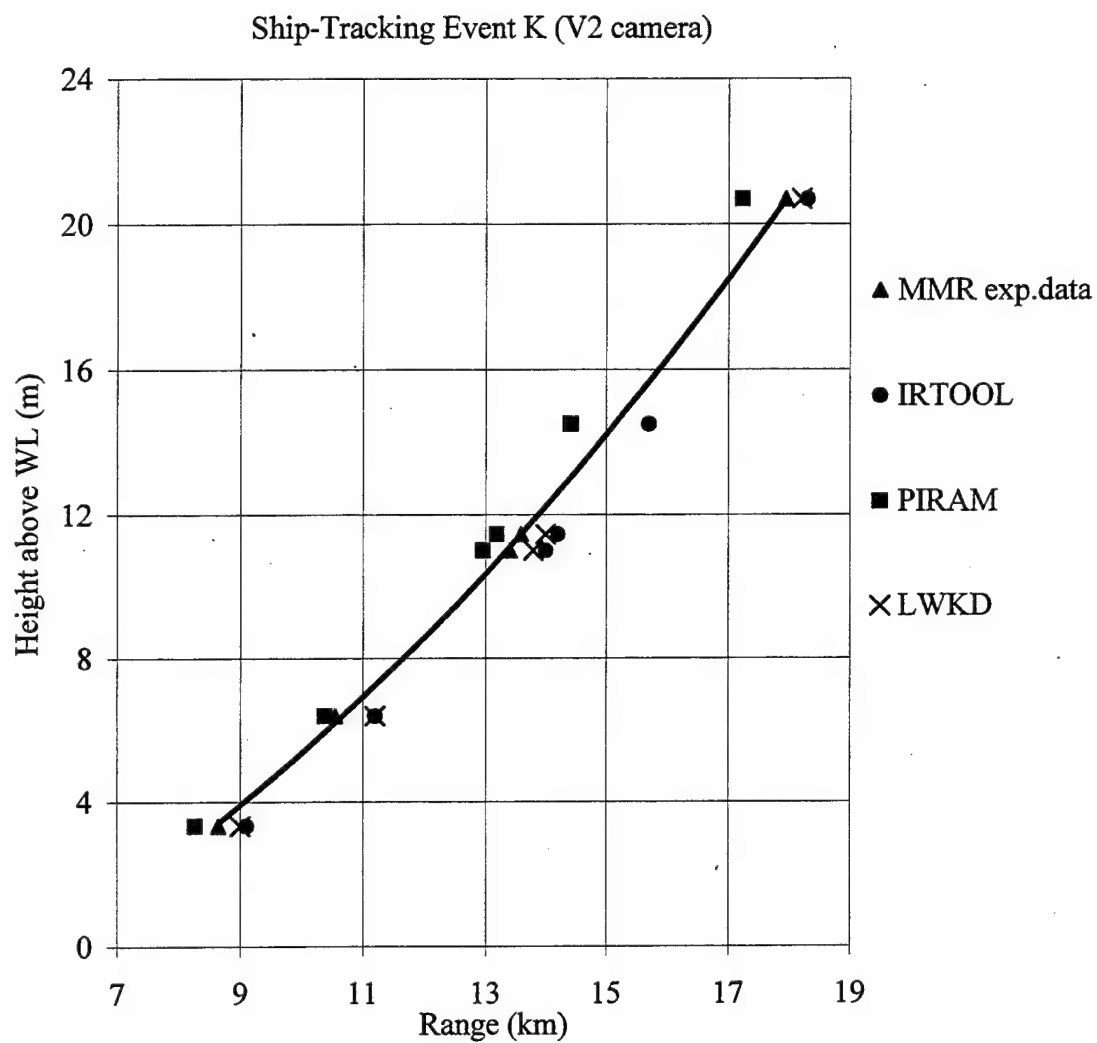


Figure 23. Comparison of the LWKD, PIRAM and IRTOOL model MMRs with the ship-tracking data measured by the V2 visible camera

Ship-Tracking Event K (V4 camera)

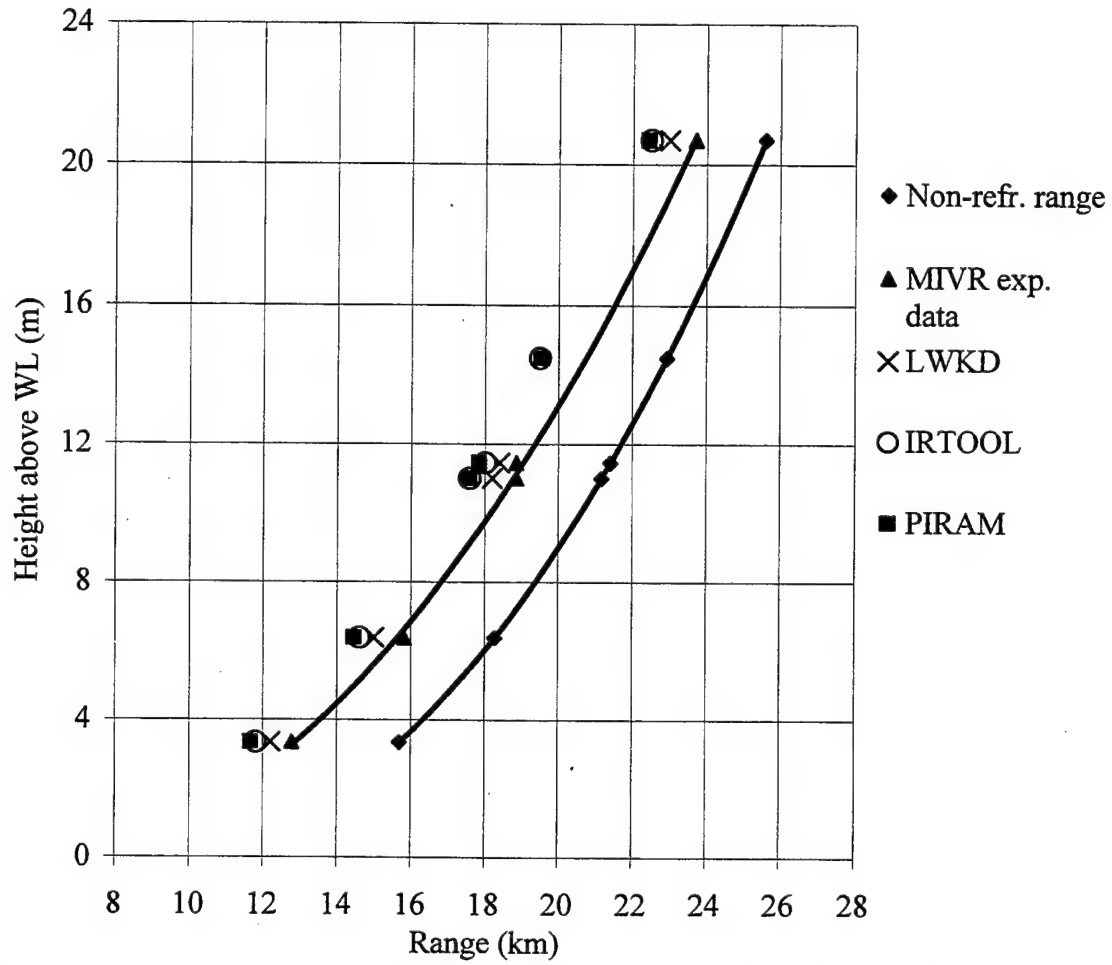


Figure 24. Comparison of the LWKD, PIRAM and IRTOOL model MIVRs with the ship-tracking data measured by the V4 visible camera

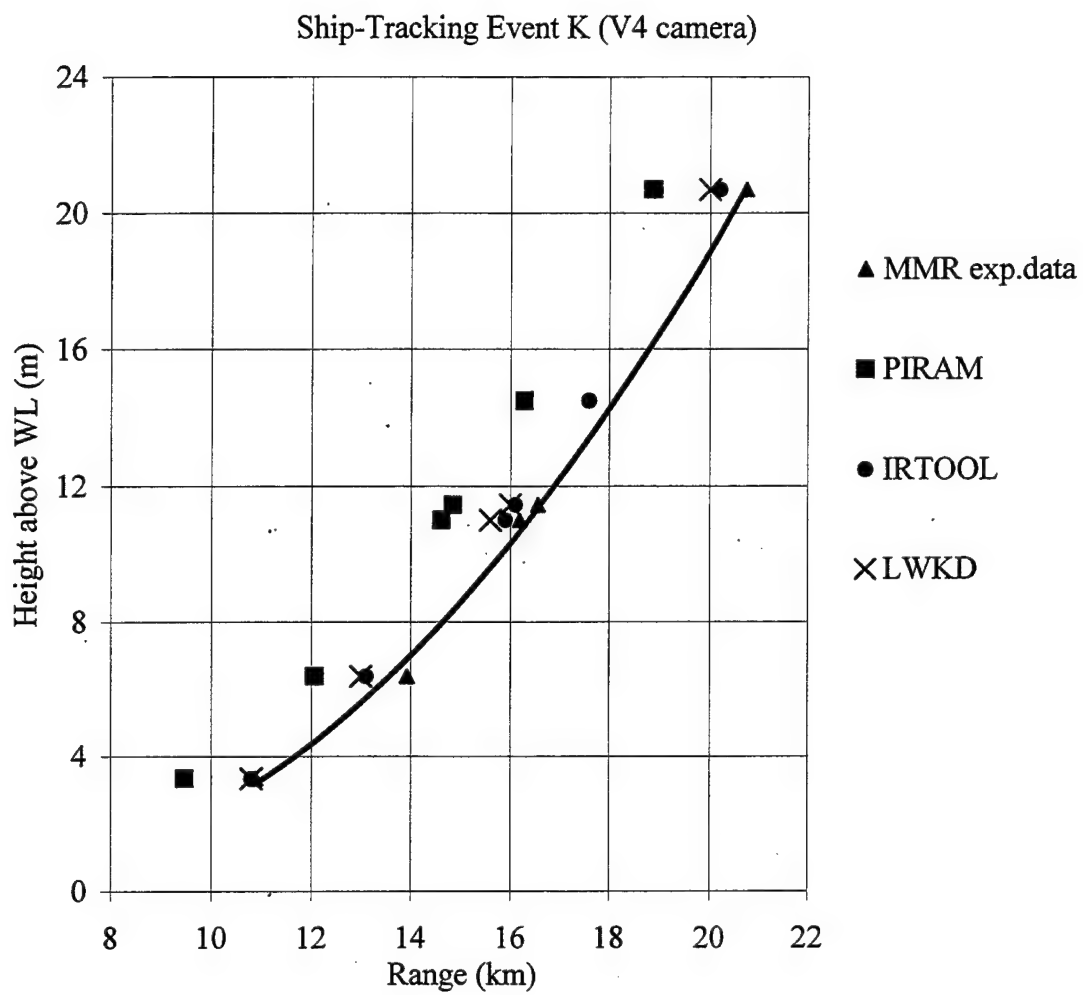


Figure 25. Comparison of the LWKD, PIRAM and IRTOOL model MMRs with the ship-tracking data measured by the V4 visible camera

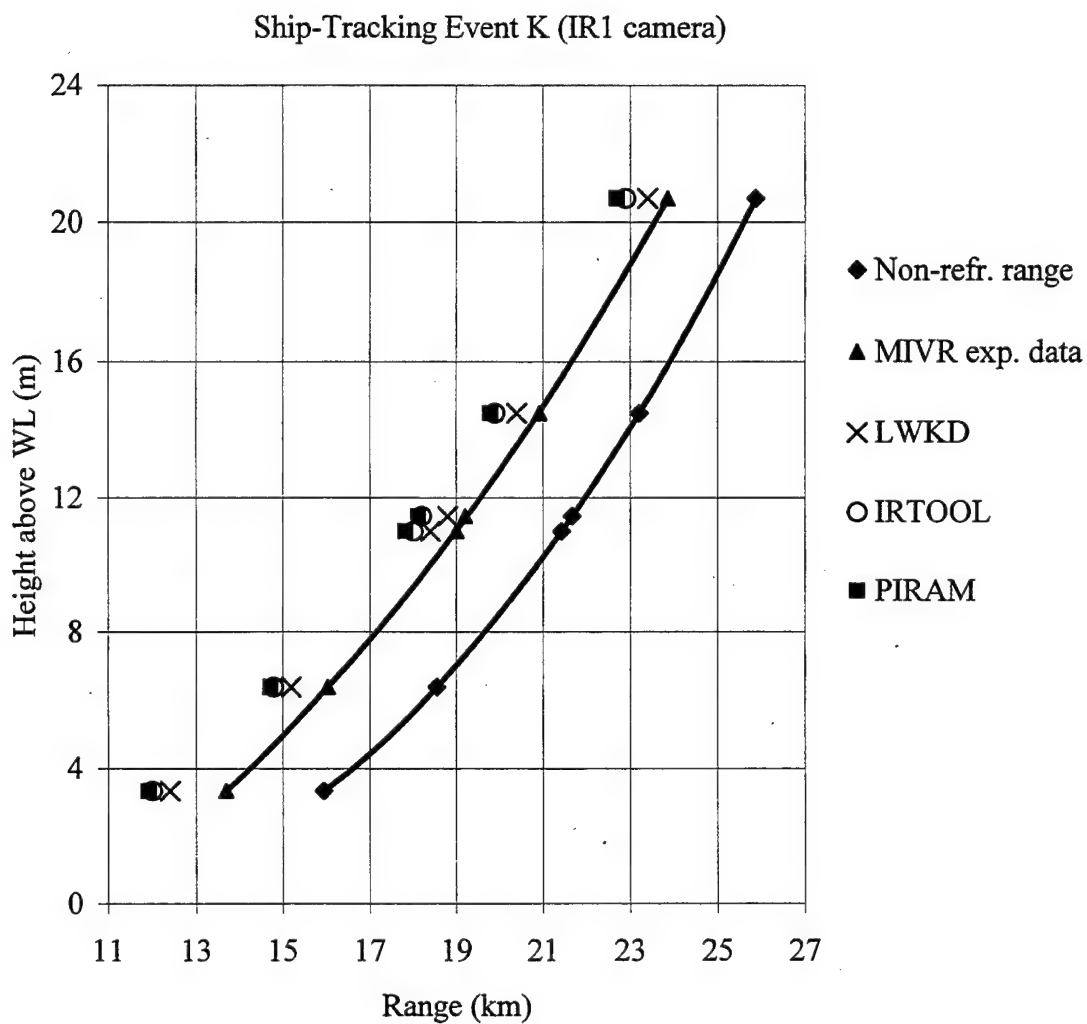


Figure 26. Comparison of the LWKD, PIRAM and IRTOOL model MIVRs with the ship-tracking data measured by the IR1 (3-5 μ m) infrared camera

Ship-Tracking Event K (IR1 camera)

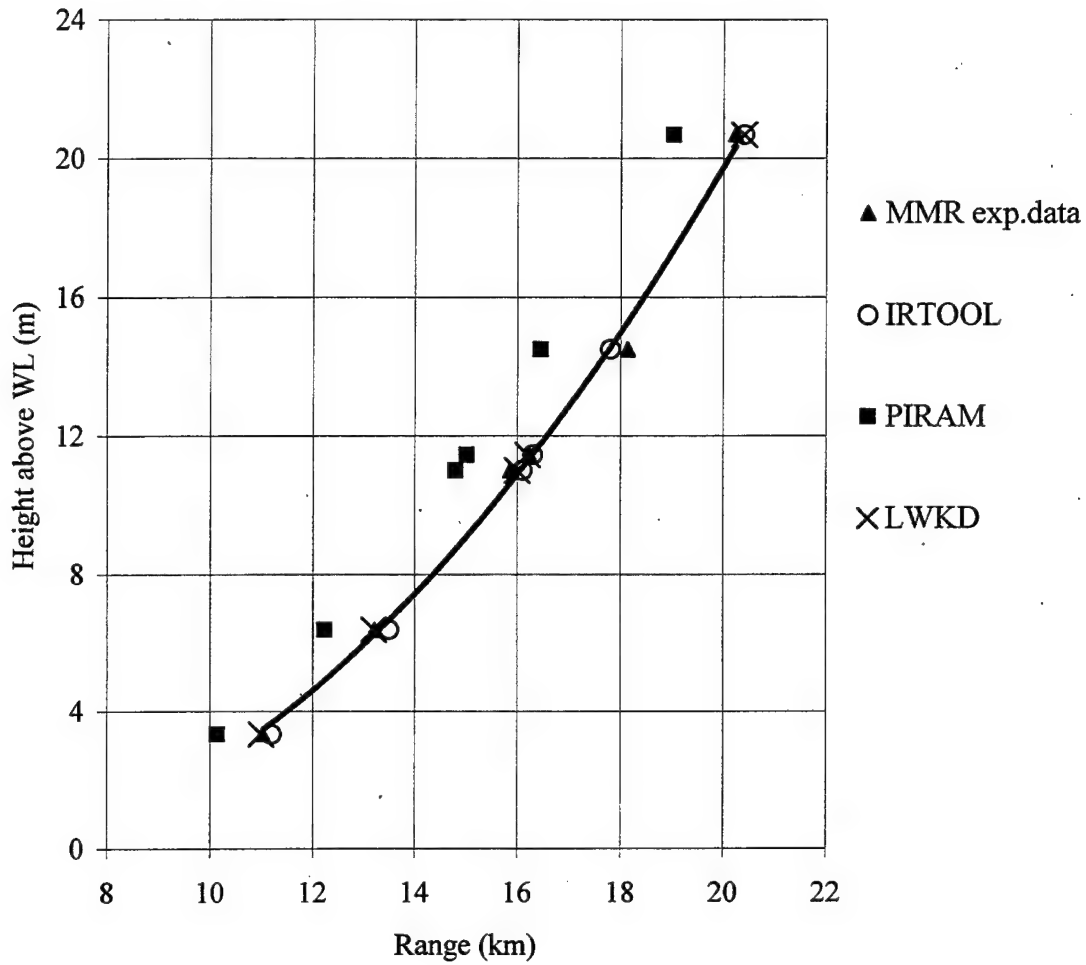


Figure 27. Comparison of the LWKD, PIRAM and IRTOOL model MMRs with the ship-tracking data measured by the IR1 (3-5 μ m) infrared camera

0.9 to 1.7 short of the experimental data. Finally the IRTOOL predicts ranges that match perfect or they are within 0.4 km of the experimental data.

Figure 28 shows the results of the model comparison for the data observed by the IR2 (8-12 μ m) infrared camera ($h_s = 8.37$ m). The solid and empty circles ('●' and 'O') represent the IRTOOL calculated MMRs and MIVRs respectively and the solid lines that connects these points are a 2nd order polynomial fit. All three model predictions agree that the MIVRs must be 3 to 4 km short of the non refractive horizon. The only experimental data MIVR point shown in this figure is the ship's stack and shows that the model predictions are about 1 km short. No mirages were observed. The most probable reason for the lack of experimental data points is the poor resolution of the camera (139 μ rad/pixel) and that the source is rather weak to be tracked by the camera at the range of the experiment.

The results of the model comparison for the data observed by the V3 ($h_s = 21.58$ m) visible camera are shown in Figures 29 to 30. All models predicted ranges that do not agree with the experimental data. The LWKD predicts MIVRs that are 2.7 to 3.3 km longer than the experimental data, the PIRAM results are 1.6 to 2.5 km longer, and the IRTOOL results are 1.9 to 2.7 km longer. The MMRs predicted from LWKD are 3 to 3.6 km longer than the experimental data. PIRAM predicts MMRs that are 1.4 to 2.1 longer than the experimental data. Finally IRTOOL predicts MMRs that are 3.0 to 3.6 longer than the experimental data. It must be mentioned here that in all previously released reports on MAPTIP results [Ref.1, Ref.12] the comparison results for the data observed by the V3 visible camera placed at high altitude (above 20 m) were disregarded. Instead the authors added the comparison results for

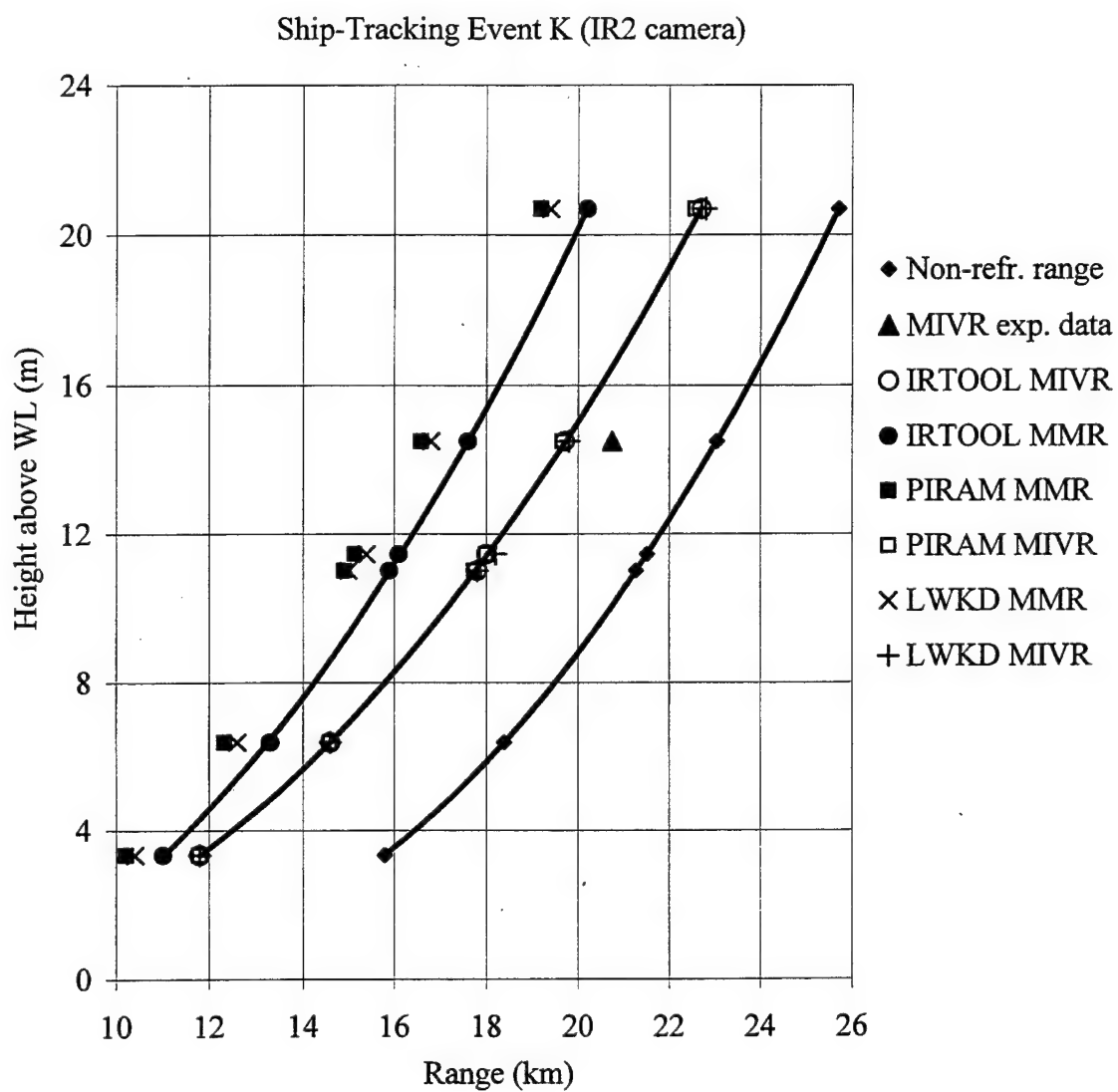


Figure 28. Comparison of the LWKD, PIRAM and IRTOOL model MIVRs and MMRs

Ship-Tracking Event K (V3 camera)

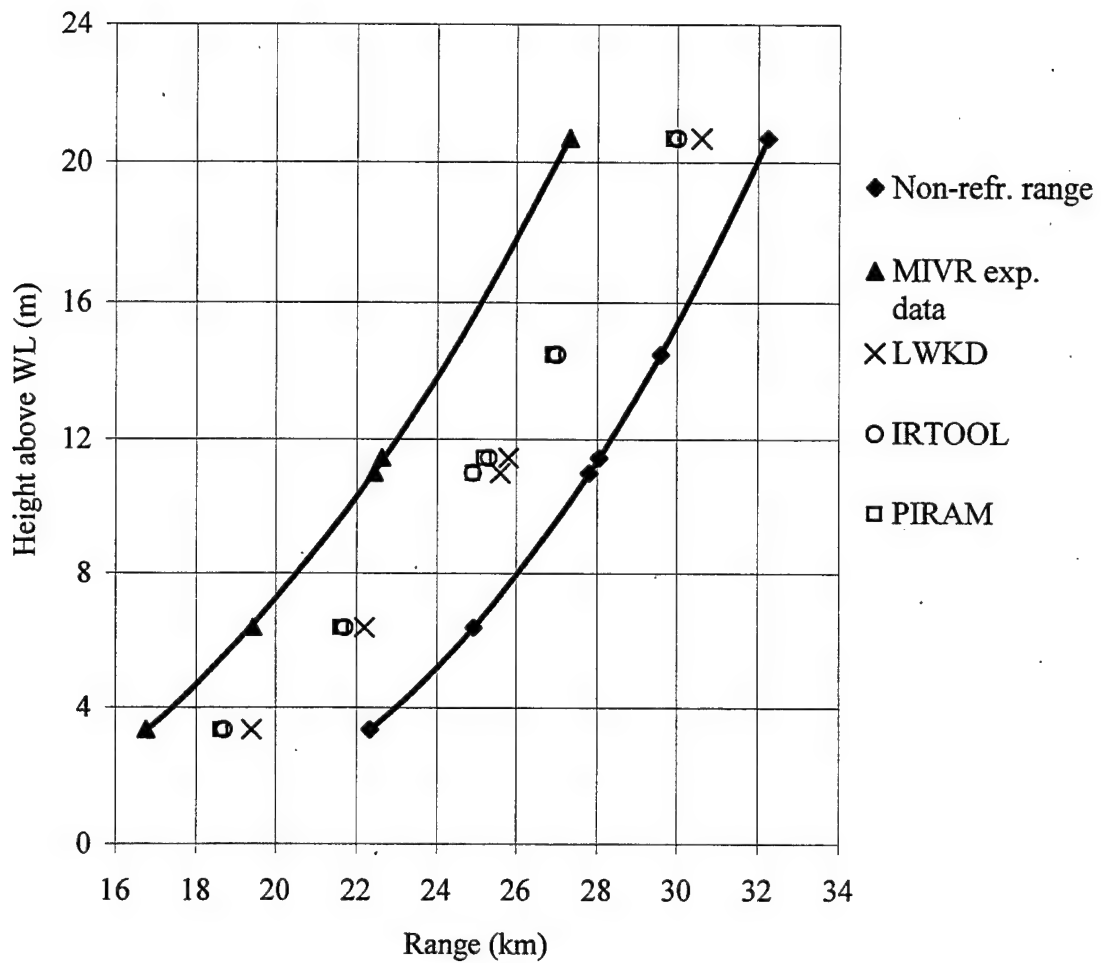


Figure 29. Comparison of the LWKD, PIRAM and IRTOOL model MIVRs with the ship-tracking data measured by the V3 visible camera

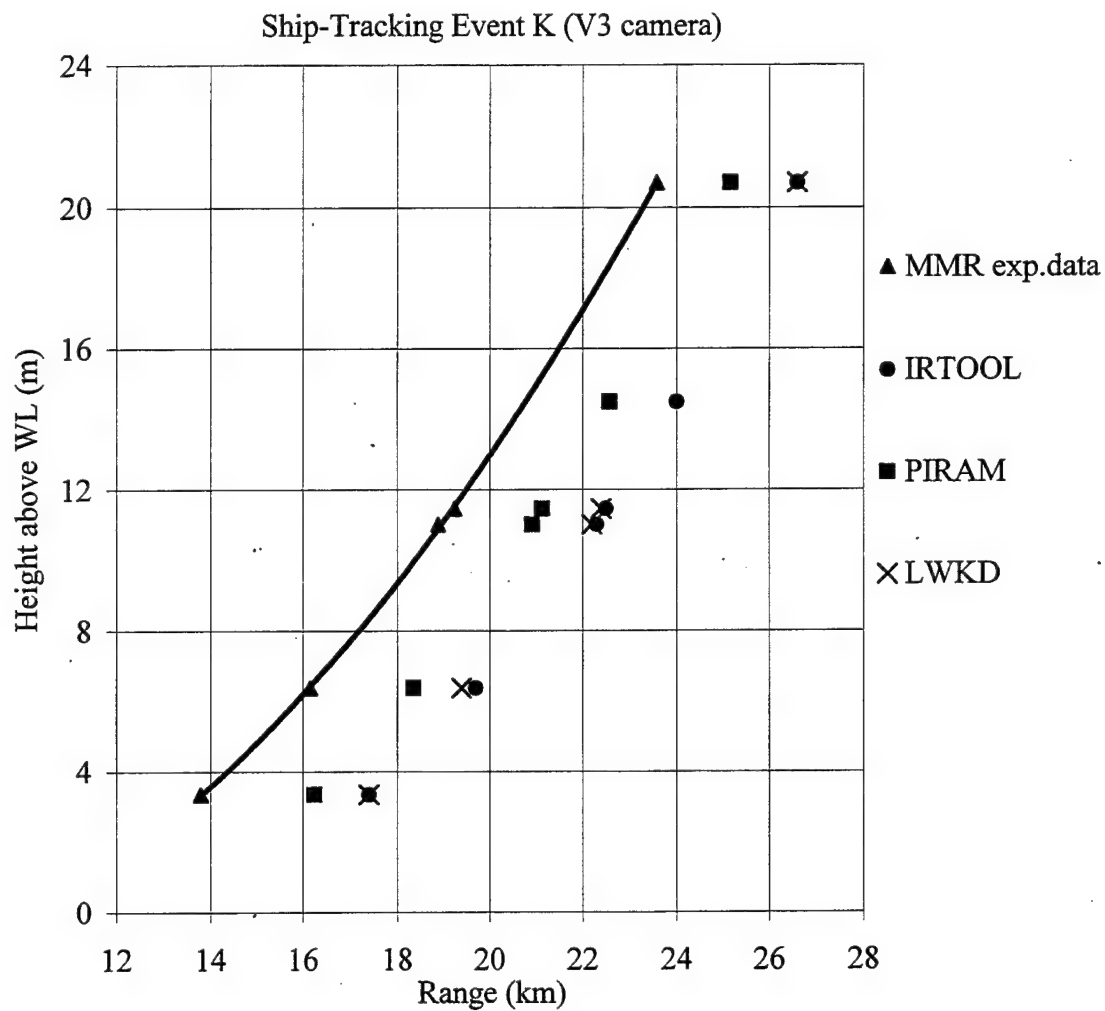


Figure 30. Comparison of the LWKD, PIRAM and IRTOOL model MMRs with the ship-tracking data measured by the V3 visible camera

the camera placed at a lower altitude ($h_s=15$ m) accomplishing a closer fit of the calculated ranges to the experimental data.

The data of the ship tracking events B and K were the most complete for the purpose of analysis. Examining the remaining events we noticed a lack of model calculations for a number of events. For events A, C, H, I, J and L no calculations of the PIRAM model existed. For events I, J, M the calculations included only those of the LWWKD (wavy LWKD) program, a modification of LWKD program. For event I, IRTOOL calculations agreed to a satisfactory level with experimental data, but for event D it did not predict mirage under conditions in which mirage was observed and the other models gave consistent results.

Finally, a significant difference was noticed not only between experimental data and the IRTOOL predictions but also between the experimental data and the LWKD or PIRAM computations. During the ship tracking events F and H in a number of cases the experimental data showed that no mirage was observed, although mirage was predicted by the LWKD and PIRAM models [Ref. 13].

IV. CONCLUSIONS

This research showed that prediction of behavior of optical/IR rays in the MBL can be achieved. The evaluated models calculated the MIVRs and MMRs of targets with some success.

The objectives of the thesis were accomplished by generating mirages in the IRTOOL program, and comparing with the calculations of other models and with the available experimental data. The suggestion that IRTOOL cannot predict mirages proved to be inaccurate. IRTOOL generated mirages in most of the sub-refractive situations in which they were observed. However in some conditions it predicted a minimum range of mirage appearance somewhat greater than found experimentally and in a few cases did not predict mirage at all. The generated Maximum Inter-vision Ranges deviated from the measured ones by typically 5 to 20%.

The comparison of IRTOOL, LWKD, and PIRAM model predictions showed similar threshold conditions (Minimum Mirage Range) for onset of mirage effects, but, with differing offsets from the observed thresholds. The thresholds are displayed as range vs sensor elevation plots. In a number of the sub-refractive cases studied IRTOOL overestimates the MMR indicating a range target distance in which mirage is observed but not predicted by IRTOOL. This distance interval is generally about 2 km, or about 10% of the detection range. This suggests a possible shortcoming of the theoretical profile generating code. Verification of this hypothesis would require very detailed comparison between IRTOOL

generated profiles and experimental data. The observed overestimation cannot be compensated by a small change in Air-Sea Temperature Difference, such as could be generated by the time/position relationships of the temperature measurements.

The comparison among IRTOOL, LWKD and PIRAM models showed that for sub-refractive conditions these programs produced mirage but were inconsistent when the sensor heights were above 20m. For heights above this level the models behaved poorly, predicting detection ranges deviating far from measurements. The expected installation of future IRST under development on AEGIS class cruisers and destroyers and other warships at heights well above 20 m makes model accuracy a critical factor for the continuation of the IRSTs development and refinement, as well as for the incorporation of an IRST performance prediction code into the AEGIS system. The models tested were also not consistent in some cases, in which they failed to predict the absence of mirage seen in the experimental data.

As mentioned in Chapters III and IV, the IRTOOL program is a combination of a MBL model and a ray tracing program. However, the LWKD and PIRAM programs are MBL models which create the atmospheric profile and then use other ray tracing programs to generate the desired calculations. As a method of evaluating or diminishing the possible differences in the different ray-tracing programs, it is recommended to use the output atmospheric profiles of each model as input to a common ray tracing program, such as the atmosphere effects module of IRTOOL. This constitutes a recommended extension of the present work. A requirement of this method is the provision of the source codes of the

models by the corresponding research organization/institute in order to evaluate whether any deviations are due to the MBL model or to the ray tracing programs.

The models that we compared use similarity theory and utilise the logarithmic temperature profiles created by the model to predict refraction of optical/IR rays. According to previous research [Ref.15] these models are valid for heights several significant wave heights above ocean surface waves because similarity theory creates extreme temperature gradients which are inversely proportional to the height z . These large calculated temperature gradients generate large refractive index gradients which result in excessive ray bending near the sea surface, that is contradictory with experimental observations. However, the agreement of the model calculations and the experimental data from the MAPTIP experiment showed a significant number of cases in which we had reliable results. Also the fact that the calculated MMRs and MIVRs are not always shorter than the experimental data contradicts the finding that, due to the excessive ray bending in the sub-refractive atmosphere, the calculated detection range is smaller than the observed one[Ref.15].

The inconsistency of the compared models accurately to calculate the detection ranges for sensors above 20m dictates the conduct of further, more realistic experiments with sensor heights above 15-20 m. Because there is no experimental confirmation of the gradient singularity in the MBL, future experiments should be focussed on verifying that the atmospheric profile in the lower 10 m of the MBL and the logarithmic form created by a model are identical.

The secondary objective of this work, which is “the inclusion of new sensor models in IRTOOL including a generic common module FLIR, and new targets including ones appropriate to low flying missiles” cannot be accomplished in this thesis. The creation of these models requires advanced programming skills and knowledge of IDL or FORTRAN programming languages in order to take advantage of the user module capabilities and can be a future project by itself.

Conducting extensive experimental measurements and data analysis will contribute to the investigation of the refractive limitations. Further refinement of the existing models will satisfy the necessity for prediction of IRST system effectiveness and simulation of their operation and will allow their development, a great challenge for the researchers in the years to come.

LIST OF REFERENCES

1. L. Forand, "The L(W)WKD Marine Boundary Layer Model," Defence Research Establishment Valcartier R-9618, March 1996.
2. L. Forand, "Marine aerosol properties and thermal imager performance (MAPTIP): refractive effects in the visible and IR," Defence Research Establishment Valcartier, Canada, 1996 in *Image Propagation through the Atmosphere, SPIE Proceedings*, Vol 2828.
3. L. Forand, D. Dion, and J. Beaulieu, "Marine aerosol properties and thermal imager performance (MAPTIP): Canada's Measurements of Refraction effects" in *Propagation Assessment in Coastal Environments*, AGARD Conference Proceedings 567, 1995.
4. "IRTOOL Atmosphere Modeling", Areté Report ARW-96-303-002-TR, October 1996.
5. R.Greenler, *Rainbows, halos and glories*, Cambridge University Press, 1980.
6. Hecht, *Optics*, Addison-Wesley Publishing company, 2nd Edition, May 1990.
7. D.Dion, "Refraction Effects on EO system detection ranges in coastal environments" in *Propagation Assessment in Coastal Environments*, AGARD Conference Proceedings 567, 1995.
8. D. C. Williams and H. Kahmen, "Two Wavelength Angular Refraction Measurement" in *Geodetic Refraction: Effects of Electromagnetic Wave Propagation Through the Atmosphere*, Springer-Verlag Berlin Heidelberg New York Tokyo, 1984.
9. A. W. Cooper and E. C. Crittenden, Lecture notes from PH 4253, *Electro-optic Sensors and Systems*, Naval Postgraduate School, Monterey, California, September 1998.
10. M. I. Skolnik, "Propagation of Radar Waves" in *Introduction to Radar Systems*, McGraw Hill, 2nd Edition, 1980.
11. K. L. Davidson, Lecture notes from MR 2416, Meteorology for Electronic Warfare.
12. L. Forand, D. Dion, Y. Hurtaud and K. Stein, "MAPTIP Workgroup report: Refractive effects in the visible and the Infrared," Defence Research Establishment Valcartier, Canada, June 1997.

13. L.Forand, Summary data for the tracking runs of the Hr. Ms. Tydeman during MAPTIP experiment (Personal communication).
14. IRTOL Reference Manual Version 2.0.0, Areté Associates (P.O. Box 6024 Sherman Oaks, CA 91413), November 1995.
15. M. Mermelstein, E. Takken, R. Priest, E.Stone, and T.Thorpe, "Target Detection and Wave Obscuration at the Ocean Horizon," Naval Research Laboratory, Washington, D.C.
16. W. G. Rees, C. M. Roach, and C. H. Glover, "Inversion of the atmospheric refraction data" in *Journal of Optical Society of America*, A Volume 8, Number 2, February 1991.
17. Press, W. H., B. P. Flannery, S. A. Teukolsky, and W, T. Vetterling, *Numerical Recipes*, Cambridge University Press 1986.

INITIAL DISTRIBUTION LIST

	No. Copies
1. Defense Technical Information Center.....2 8725 John J. Kingman Rd., STE 0944 Ft. Belvoir, VA 22060-6218	
2. Dudley Knox Library.....2 Naval Postgraduate School 411 Dyer Rd. Monterey, CA 93943-5101	
3. Chairman, Code PH.....1 Department of Physics Naval Postgraduate School Monterey, CA 93943-5121	
4. Professor Alfred. W. Cooper, Code PH/Cr.....2 Department of Physics Naval Postgraduate School Monterey, CA 93943-5121	
5. Professor David D. Cleary, Code PH/Cl.....2 Department of Physics Naval Postgraduate School Monterey, CA 93943-5121	
6. COMMANDING OFFICER.....1 SPAWARSYSCEN SAN DIEGO ATTN: Dr. D. R. Jensen, D883 49170 Propagation Path, San Diego, 92152-7385	
7. NAVAL SEA SYSTEMS COMMAND.....1 PEO Theater Air Defense, Ship Self Defense, ATTN: Mr. J.E. Misanin, PEO-TAD D234, Washington, DC 20363-5100	
8. Embassy of Greece.....1 Naval Attache 2228 Massachusetts Avenue, N.W. Washington, DC 20008	

9.	Antonios Georgopoulos.....	3
	Platonos 28B	
	Galatsi 11147	
	Athens	
	GREECE	